UNIVERSITÀ DEGLI STUDI DI PADOVA

Dipartimento di Fisica e Astronomia
Corso di Laurea in Astronomia

Tesi di Laurea Triennale

Volcanism and Cryovolcanism in the Solar System: from Mercury to Charon

Relatore:
Prof.
Stefano Casotto

Candidato:
Alessandro Ruggieri
Matricola: 1100366

Anno Accademico 2017-2018

Contents

Introduction

Volcanic and cryovolcanic phenomena are quite common in the Solar System, among rocky planets and satellites. Studying this kind of phenomena is particularly important, because it gives us an insight about the internal composition and activity of these bodies. These information are especially useful to determine how our Solar System formed and evolved in the distant past. However, it is important to distinguish between volcanic and cryovolcanic phenomena. The former are typical of the terrestrial planets, where temperatures are relatively high and heavy elements are present, whereas the latter characterize the icy satellites of the giant planets, where low temperatures and different chemical compositions do not allow phenomena involving lava. Volcanism is defined as the phenomenon of eruption of molten rock (magma) onto the surface of a solid-surface planet or moon, where lava, pyroclastics and volcanic gases erupt through a break in the surface called a vent. Cryovolcanism is defined as the eruption of liquid or vapor phases of water or other volatiles that would be frozen solid at the normal temperature of the icy satellites' surface. As pointed out by these definitions, the two main differences between these phenomena are the temperatures involved and the chemical composition of the materials that are brought to the surface. However, they both require some sort of heating process. The main processes that can generate the required heat are: accretion (the kinetic energy of the planetesimals is converted into heat), the decay of short-lived radioactive isotopes (which provides heat during the first 10 Myr following accretion), the decay of long-lived radiogenic isotopes (which can provide heat for several billion years), and tidal dissipation, which causes orbital evolution and changes in the total energy. It is also important to understand how this heat is brought towards the surface. This is due to different processes, such as conduction and convection.

The purpose of this work is to provide some insight on the main volcanic and cryovolcanic processes found in the Solar System, and the possible mechanisms that drive these processes. In the next chapters, evidence for volcanic or cryovolcanic activity on several bodies of the Solar System will be discussed. Several model will also be explained, in orded to provide an explanation of how volcanic and cryovolcanic processes work on these bodies. The result is that volcanic and cryovolcanic processes are present wherever some sort of heating process is present, such as tidal heating or the decay of radiogenic isotopes.

In Chapter 1, volcanic activity on the terrestrial planets will be considered and it will be illustrated that it is definitely present today on Venus and Mars. In Chapter 2, volcanic activity on Io will be explored through the analysis of different rheological models that have a strong influence on how this satellite evolved. In Chapter 3, it will be shown how the atmosphere and surface of Titan prove that both volcanic and cryovolcanic processes must have taken place on this satellite. In Chapter 4, the observed cryovolcanic activity on Enceladus and a model for the internal structure will be explained. In Chapter 5, the spectra of Charon's surface will be discussed, demonstrating that cryovolcanism is the only kind of process that can explain the presence of crystalline water ice. In Chapter 6, the evidences for the presence of cryovolcanic activity on other relevant satellites of the Solar System will be discussed, illustrating that this kind of phenomena is common in the whole Solar System. The result is that volcanic and cryovolcanic processes are present wherever some sort of heating process is present, such as tidal heating or the decay of radiogenic isotopes.

Chapter 1

Terrestrial planets

The purpose of this chapter is to provide proofs which demonstrate that volcanism happened on terrestrial planets. On Mercury, this is thought to have happened only in the distant past, while Venus and Mars were active in the geologically recent past and may still be active today. Information taken from G. Faure and T. M. Mensing, Introduction to Planetary Science [56].

1.1 Mercury

Several craters on Mercury's surface show evidence of ancient lava flows. Since some regions have been resurfaced by these lava flows, the impact craters are not uniformely distributed. The great number of craters on the surface of Mercury demonstrates that this planet underwent a heavy bombardment soon after its formation. This proves that the volcanic activity occured after the period of intense bombardment, which ended at about 3.8 Gyr. The core of Mercury is tought to be solid due to the surface-to-volume (S/V) ratio of the planet, which is similar to those of Mars and the Moon, both with a solid core. Therefore, the high S/V ratio predicts that Mercury, just like the Moon and Mars, is geologically inactive at present time. Presumably, the volcanic rocks on Mercury's surface are 3.0 to 4.0 Gyr old, which means that the heavy bombardment caused the crust to shrink and form scarps from which lava could actually escape [196]. In particular, there are some planes with a very low albedo within craters that may actually prove that there was volcanic activity on Mercury, at least in the distant past.

1.2 Venus

1.2.1 Surface features

Venus only has a few craters and radar images prove the presence of features linked to tectonical activity: these two facts demonstrate that Venus is still geologically and volcanically active today. In fact, most of Venus' mountains are volcanoes, the chasmata are deep trenches formed by tectonic processes in the mantle of Venus, coronae are the surface expressions of convection currents in the mantle and appear to be the sources of basalt lava, and finally the northern highlands are partly surrounded by low-lying lava plains called planitiae, which are the lowest areas in terms of altitude. The lowest areas on Earth are the basaltic floors of the oceans, but they are very different from the planitiae, which appear to have experienced strong deformation. Even if subduction of lithospheric plates probably never happened on Venus, there are features which resemble subduction zones on Earth and which are found close to several volcanoes in Aphrodite terra, near the equator. Other volcanoes are found in regiones south of Guinevere and Aino planitiae. The resulting image of Venus is that of a geologically active planet with tectonic processes still going on.

1.2.2 Volcanic activity

Even if none of Venus' volcanoes erupted during our observations, radar data prove the existence of relatively recent volcanic activity. The slope of Maat Mons is covered by lava flows that reflect radar waves efficiently, suggesting that they are younger than 10 Myr [61]. On Venus, several lava domes can be seen: they are features about 1 km high and 100 km wide, occur in clusters and presumably formed by the extrusion of viscous magma from subsurface magma chambers. However, the lava that formed these domes seems to be very different from the low-viscosity and basaltic one that formed the rocks seen in the low plains. On Venus there are more than 200 channels, which are very similar to Earth's rivers, but they do not posses tributaries and are narrower, some of them have deltas, most of them are more than 500 km long and are very smooth, the width decreases from the source to the end and some of them split into two or more distributaries. Low-viscosity lava spread globally throught these channels, acting like water does on Eart, and it this is the only way to explain the uniform length of these channels. The length of the channels confirms the low viscosity and makes them similar to those found on the Moon and on Mercury. Some of the analyzed rocks are similar to the basaltic ones on Earth, but those found in the lava domes have unknown composition, so apparently there are two kinds of rocks on Venus.

Volcanism is a way in which terrestrial planets transport heat from the interior to the surface, where it is radiated away: on Earth [238] 20 km^3 of basalt lava are produced annually, while on Venus, only 1 km^3 of basalt lava is produced every year, so this planet loses much less heat than Earth. Since the two planets must have very similar heat productions, but Venus emits between 10 and 30 mW m^{-2}, whereas Earth emits 84 mW m^{-2} [243] the conclusion in that Venus' mantle is heating up and this will lead to another major resurfacing, similar to the one that happened 750 Myr ago [234, 169].

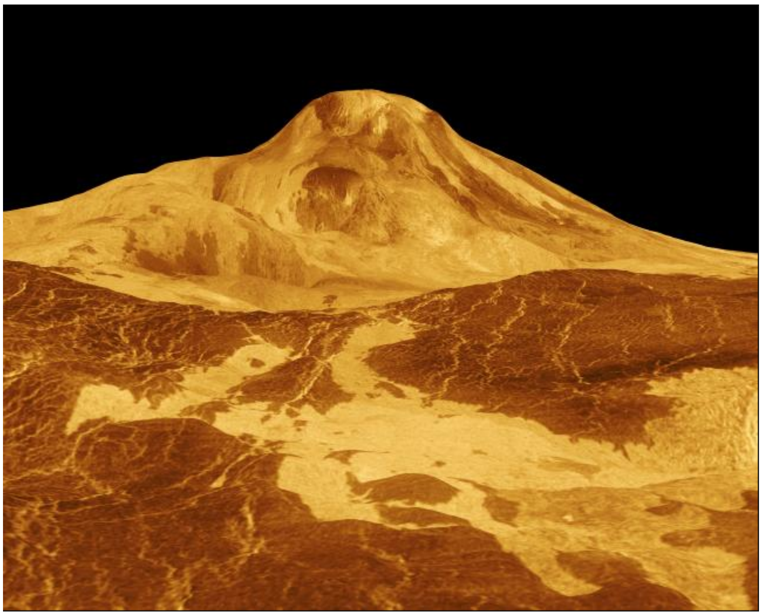

Figure 1.1: Maat Mons on Venus. As mentioned in Section 1.2.2, this mountain has been proven to be younger than 10 Myr and is therefore one of the youngest parts of Venus' surface.

1.2.3 Episodic resurfacing

The craters are uniformally distributed, so the whole surface has the same age of 500 Myr, but the craters are very large due to the dense atmosphere. Like on Earth, rejuvenation of the surface occurs on Venus but, unlike on our planet, here it seems to occur episodically and globally. On both planets, there is convection in the form of plumes that rise from depth and cause volcanic activity on the surface, although the basaltic crust of Venus is not being subducted into the mantle. It seems that Venusian volcanoes remained dormant for several 10^2 Myr, until the high temperature created a crack in the litosphere from which lava could escape and spread globally, rejuvenating the surface and generating the volcanic rocks seen today. The process ended with the formation of a new crust by crystallization of the basalt lava exposed at the surface. Afterward, some volcanoes remained active for some time until volcanic activity ceased completely. This theory explains the random distribution of impact craters and the uniformly low age of the surface, but raises a question about the thickness of the lithospheric mantle. This hypothesis assumes that Venus has a 300 km thick lithosphere which prevents continuous volcanic activity, but the estimate of the temperature gradient in the crust and the evidence of crustal deformation by compression and extension suggest that Venus has a thin lithosphere. Even the apparent absence of plate tectonics can be attributed to the mechanical weakness of a thin lithosphere that cannot withstand the stresses applied by convection in the asthenospheric part of the mantle. Earth has 120 km-thick litospheric plates and a temperature at that depth of about 1300 °C [254], therefore the temperature gradient is about 11 °C/km (assuming 0 C at the surface). On Venus, the surface temperature is 460 °C, so the temperature is 1760 °C at a depth of 120 km. If the properties of rocks in the mantle change from lithospheric to asthenospheric at about 1300 °C, then the lithosphere of Venus is only about 76 km thick. Similar results were obtained by other investigators who used geophysical modeling [169, 80, 124]. The problem concerning the thickness of Venus' lithosphere can be resolve by seismic data, which are not avaiable because of the difficult environmental conditions of the surface.

1.3 Mars

1.3.1 Surface features: northern hemisphere

Tharsis Plateau

The Tharsis plateau is an area that rises to an elevation of about 7 km above the zero-elevation contour, that occupies the region from 40 °S to 50 °N and from 60°W to 140 °W, and contains several high volcanoes, of which the highest one is Olympus Mons, whose summit has an elevation of 21287 m. This area is younger than 3.8 Gyr, as shown by the low crater density, is formed of basalt lava, which has low viscosity, and some lava flows within it appear to be younger than 160 Myr. This plateau could have formed due to a plume at the base of the litosphere, in which the plume formed a dome, increasing the temperature and causing the rocks to expand, forming fractures that became rift valleys through which lava, given by decompression melting of rocks, could leak. Therefore, the three principal shield volcanoes (Arsia, Pavonis and Ascraeus) could be aligned because the magma that fed them reached the surface by means of the same fractures system, and the fact that other volcanoes are located along the extension of the chain of the principal volcanoes supports this theory. The Tharsis plateau is surrounded by a radial system of rift valleys: some of them reach the ancient highlands of the southern hemisphere, the others pass through the surrounding planitiae and reach the north-polar desert.

Olympus Mons

Olympus mons is the largest volcano of the Solar System, with an elevation of 21287 m above the zero-elevation contour and a diamater of about 600 km at its base. The summit plateau contains a gigantic caldera which is 70 km wide and 3 km deep. The slopes are covered by several layers of lava flows and the younger one is about 10 Myr old, but the amount of lava seen suggests that it has been active for several 10^2 Myr and it may also erupt again in the future [83].The Olympus mons is surrounded by a cliff (up to 6 km high) that was either formed by wave erosion (i.e., it is a sea cliff), or by the eruption of lava flows within an ice sheet [111]. Olympus mons presumably formed due to a large mantle plume that formed magma which rose to the surface through fractures in the lithosphere and crust, building up the modern mountain. This process is similar to the one that formed Mauna Loa (Hawaii), with the difference that Olympus Mons is much higher because Mars does not have plate tectonics and therefore, unlike Mauna Loa, it remained above the plume and was supplied with more magma. This is considered the proof that Mars does not have plate tectonics, otherwise Olympus Mons would be much lower.

Young lava flows

Using the images returned by the Mars Global Surveyor [82], it has been determined that the exposure age of the lava flows of Elyseum mons lies between 600 and 2000 Myr. Some lava flows in these planitiae that may even be less than 100 Myr old [83]. Some flows on Olympus Mons and on the Amazonis and Elysium planitiae are thought to be as young as 10 Myr. The isotopic age determinations of basaltic martian meteorites indicates that they crystallized between 154 and 474 Myr. These fact seem to suggest that Mars is still active today, but this is in constrast with the high surface-to-volume ratio of the planet, which should indicate that Mars has cooled more rapidly than the Earth and Venus.

1.3.2 Surface features: southern hemisphere

The southern hemisphere is much more cratered than the northern one, although there are several younger volcanoes and some craters appear to have been covered by sediments deposited by water and/or wind. The geologic evolution of Mars can be divided into three intervals of time. During the Noachian Eon (4.6 to about 3.5 Ga), there were many impacts, while global volcanic activity was going on, liquid water eroded the surface and transported sediments, while the denser atmosphere caused a light greenhouse effect. During the Hesperian Eon (3.5 to about 2.5 Ga), the atmosphere

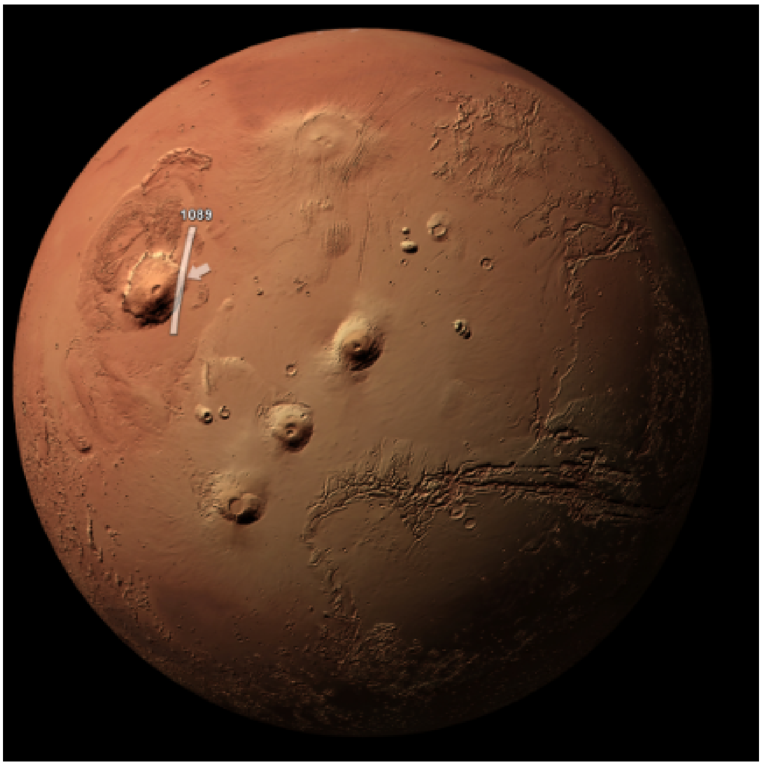

Figure 1.2: The most impressive volcanoes of Mars. The biggest one is the Olympus Mons, which is the biggest known mountain of the Solar System, the other three are the Arsia, Pavonis, and Ascraeus Montes. Other smaller volcanoes can also be seen.

became thinner, decreasing the temperature, while volcanic activity and the volume of erupted lava declined and ice formed on the surface, especially at the poles. During the Amazonian Eon (2.5 to 0 Ga), volcanic activity ceased, except for rare localized eruptions of lava (probably the Amazonis planitia). The dates are based on the number of craters per unit area and, to a much lesser extent, on the results of isotopic dating of martian meteorites that have been found on the Earth [83]. Due to the low atmospheric pressure, water cannot be liquid on Mars, but solid water is found under the surface and in the polar regions.

1.3.3 Volcanoes of the southern hemisphere

In the southern hemisphere there are several craters as well as several traces of global volcanic activity. A large shield volcano called Syrtis Major forms a prominent landmark about 600 km west of the Isidis basin, towards which lava flowed from the two calderas found at the summit of the volcano, and the low crater density of the lava flows suggests that this happened after the

Isidis basin had formed. This volcano is thought to have formed during the Hesperian age, because it is found above ancient highland terrain, suggesting that Mars was still active at that time (less than 3.8 Gyr ago). The southern hemisphere contains additional evidence of relatively recent volcanic activity at Hespera planum (22 °S, 254 °W). This high plane in Terra Tyrrhena consists of lava flows that were extruded by a large volcano called Tyrrhena patera, are very lightly craterd and formed features similar to some observed on the Moon. Close-up images of Tyrrhena patera reveal that the slope of this volcano has been dissected by a radial set of gullies with uncertain origin that can also be observed on another small volcano called Hadriaca patera, which is located about halfway between Tyrrhena patera and the northeastern rim of the Hellas impact basin. However, the Hadriaca patera seems to be composed of volcanic ash rather than of lava flows [83], as revealed by the fact that it is connected to the Niger/Dao valley siystem through a set of steep-walled canyons.

1.3.4 Mars Love number and interior

Mars is thought to have an iron core, because of the remnant crustal magnetism [2] and the polar moment of inertia [57]. The point is to determine whether the core is fluid or not, because this is linked with the possible volcanic activity. A first estimate, based on Mars Global Surveyor (MGS) and carried out by Smith et al. (2001) [215], gave $k_2 = 0.055 \pm 0.008$, which implies a solid core since $k_2 \leq 0.10$. Using later data (MGS, range and Doppler data from Viking Lander and Mars Pathfinder) concerning tides on Mars, it has been possible [256] to estimate a totally different value of $k_2 = 0.153 \pm 0.017$ (the uncertainty has been enlargened on purpose to account for model deficiencies and instrumental noise). This value includes the effects of both solid-body and atmospheric tides. The latter can be estimated through the knowledge of the semidiurnal pressure change at the surface [75]. This has been calculated using the atmospheric global circulation models (GCM) with Mars Pathfinder pressure data, leading to the estimate that atmospheric tides contribute to the value of k_2 by about 0.004 to 0.008. What's more, the Love number is increased by about 0.002 because of solid-body friction and fluid core nutation. The solid-body tides contains both elastic and inelastic components, where the former one can be compared with models [258, 69, 218, 261], while the latter depends on the tidal quality factor Q, which has been estimated, using the Phobos orbit decay, as $Q = 92 \pm 11$. Assuming that Mars behaves like Earth, the inelastic correction is 0.005 and therefore, the elastic value of k_2 for Mars is 0.145 ± 0.017.

Reconstructing Mars interior using models based on that of Earth, the value of k_2 with its uncertainty constrains the core radius R_c between 1520 km and 1840 km. What's more, the results show that Mars interior has a similar composition to that of Earth if the interior is cold and the crust is thin. If the core is partly solid, than the mantle is softer than assumed in the elastic solid model and this could explain the high value of k_2 that has been found. In particular, if the molten fraction is 5% in volume, k_2 is increased by about 10 to 15%, reducing the core radius by 100 to 150 km. In conclusion, both the observations and the calculated Love number seem to suggest that Mars may today be geologically active, in spite of the high S/V ratio. This requires some sort of heating mechanism different from the common tidal heating, since its eccentricity is apparently too low to generate it.

Chapter 2

Io

The purpose of this chapter is to describe the volcanic features on Io's surface and how rheological models describe Io's interior. The use of different models leads to differences in the possible orbital evolution. Information taken from G. Faure and T. M. Mensing, Introduction to Planetary Science [56], and J. P. Renaud and W. G. Henning (2017) [193].

2.1 Volcanoes

In spite of being similar to the Moon and with surface temperatures between -148 °C and -138 °C, Io is the most active body of the Solar System with a molten silicate core, due to the high tidal heat generated thanks to its forced eccentricity (0.004) with Europa. Observations proved that Io has more than 100 volcanoes and no craters, which are soon covered by lava as they form. It was initially believed that this lava was composed of molten sulfur, but the high temperature (1750 °C) indicates that it this is lava of molten silicates and Mg-rich basalts. Since volcanoes are distributed randomly, the mantle is currently liquid, hotter than that of Earth and, presumably, about 800 km deep. The rate of production of lava, volcanic ash, and sulfur compounds on Io is sufficient to cover its entire surface with a layer about one meter thick in 100 years. On the surface of Io there are reddish haloes composed of S_3 and S_4 [223], which together form the stable yellow form of sulfur S_8. When the hot gas emitted by plumes crystallizes, it forms sulfur dioxide snow. The material extruded solifies and makes the crust much darker than initially is.

2.2 Plumes

The plumes are umbrella-shaped fountains that are emitted at speeds from 1100 to 3600 km/h, reach heights of 500 km due to Io's low gravity and tenuous atmosphere, and consist of sulfur dioxide gas with other sulfur compounds and silicate minerals. Some plumes may be active in the same location for many years, or can be short-lived, change location, or even be invisible throughout their existence or become invisible at some point. A model that explains the mechanism by which plumes are produced is the one developed by Susan Kieffer in 1982 [252]: a deposit of sulfur dioxide snow is covered by a lava flow, increasing the temperature and vaporizing the snow, so that this gas is emitted through fractures in the lava flow generated by the increased pressure. In this way, several plumes can form at the same time or in sequence, and they remain active until the lava flow cools or until the sulfur deposit is exhausted. In this model, the invisible plumes are those generated from sources with no particulates [252]. The model can explain why some plumes are short-lived whereas others last for years, why some plumes appear to migrate, and why others are invisible. In addition, the model can explain the sulfur-cycle on Io, where subsurface reservoirs of liquid sulfur dioxide form and are later emitted as plumes [115].

2.3 Surface features

Some of the largest volcanoes on Io are associated with a plume and have developed large calderas that contain lakes of cooling lava, which can form a crust and cover the hotter lava underneath. Pele has a plume that reaches a height of 400 km, which deposited a red ring of S_3 and S_4 with a radius of 700 km from the vent, and a lava lake in its caldera exposes fresh lava for a distance of about 10 km. Loki is the most powerful volcano in the Solar System and has a caldera filled with lava that may have been erupted shortly before the flyby of Galileo on October 10 of 1999. On this occasion, the spacecraft also observed the plume of Prometheus, which had moved west of 100 km with respect to the first observation made in 1979 by Voyager 1, due to the eruption of a new lava flow that reached a new deposit of sulfur dioxide snow. The volcano Tvashtar shows several calderas with lava fountains 1500 m high, thanks to Io's low gravity and the lava's low viscosity [130], and a plume that reaches a height of 400 km and is depositing a reddish ring of sulfur. This plume is very surprising because, unlike the others, is near Io's pole, and became invisible at some point in order to be sostituted by a new one (600 km southwest) that reached a record height of 600 km. On February 21, 2002, the Keck II telescope [140] observed the output of hot lava (1230 °C) by the volcano Surt, located at about 45 °N latitude, that covered an area of 1900 km^2 and released an incredible amount of heat. Near the caldera of Tvashtar there is a flat-topped mesa which is adjacent to the lava lake and whose sides suggest that a form of mass wasting is occuring. The explanation seems to be that basalt sapping is being caused by a liquid discharged by springs at the base of the cliff. The springs may be discharging liquid SO_2 from a subsurface reservoirs, which instantly vaporizes in the vacuum. On Io there are mountains which are not volcanoes and appear to have formed due to the uplift of blocks of crust by convection currents in the underlying magma ocean of the upper mantle [150].

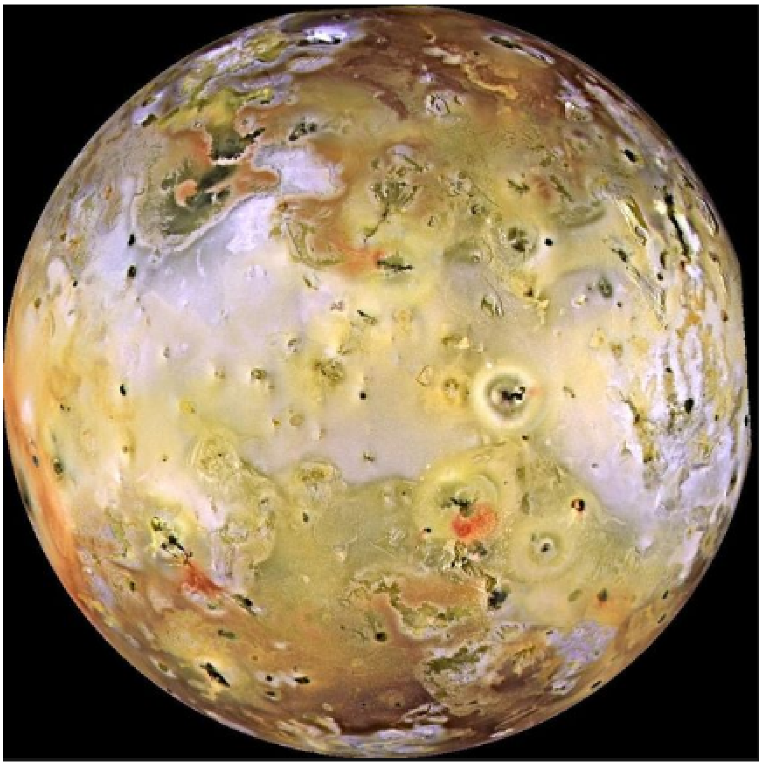

Figure 2.1: The surface of Io. The image shows the great number of volcanoes and other interesting features, such as the sulfur haloes mentioned in Section 2.1.

2.4 Introduction to rheological models

Since several bodies of the Solar System experience tidal stresses, it is important to develop models describing their interior which are based on laboratory data. The first model used for this was the Maxwell model, which only includes elastic and steady state creep response, with no transient creep regime. A first stage in improvement may be obtained by considering the Burgers rheology, which includes transient creep, but has historically had difficulty in matching Earth observations that probe the interior. Greater success has been obtained from the Andrade rheology [40, 103], in part because it is founded upon laboratory experiments, and, for this reason, a growing body of work has now applied the Andrade rheology to planetary tidal problems. The most recent model is the one proposed by Sundberg and Cooper (2010) [235], which is similar to the Andrade model and has had the same success. Here, it will be shown how the Andrade and the Sundberg-Cooper model are better than the Maxwell and the Burgers model when it comes to describe the Io-Jupiter system. Io is in a spin-orbit resonance and in orbit-orbit resonance with Europa (2:1) and Ganymede (4:1): both these effects contribute to pump its eccentricity, making tidal forces much stronger.

2.5 Analysis of rheological and thermal evolution models

2.5.1 Interior and thermal models

Following methods similar to recent studies of tidally active bodies (e.g., [91, 97, 210], the average time rate of change of the temperature of the satellite's mantle T_m and core T_C are:

$$\dot{T}_m = \frac{\dot{E}_{radio} + \dot{E}_{tidal} + Q_{CMB} - Q_{Conv}}{(S_t + 1)M_m c_m}, \tag{2.1}$$

$$\dot{T}_C = -\frac{Q_{CMB}}{M_c c_c}. \tag{2.2}$$

The Stefan number S_t can be approximated [210] by using the latent heat of the mantle $L_m = 3.2 \times 10^5$ J K^{-1} as:

$$S_t = \frac{L_m T_s}{c_m(T_l - T_s)}. \tag{2.3}$$

These temperatures are needed to calculate the viscosity and compliance (the inverse of rigidity). The terms used are: Q_{CMB} is the heat passing through the core-mantle buondary, Q_{Conv} is the total heat escaping the mantle due to convection, M and c are the masses and specific heats of the core and mantle, the mantle is heated by the decay of radiogenic isotopes, indicated by the emitted power $\dot{E}_{radio}$. The rate with which radiogenic elements are present is assumed to match that of modern Earth.
Tidal heating within the homogeneous mantle is given by [208]:

$$\dot{E}_{tidal} = -\mathrm{Im}(k_2)\frac{21(R_{sec}n)^5}{2G}e^2 f_{tvf}, \tag{2.4}$$

which is related to the forced eccentricity e, orbital mean motion n and the rheological response described by $-\mathrm{Im}(k_2)$, the imaginary part of the Love number [137][1]. The tidal volume factor $f_{tvf} = V_{mantle}/V_{planet}$ [91] accounts for the fact that tidal heating is focused within the mantle and not the core [90]. Heat is assumed to be transported out of the core into the mantle, and later out of the mantle to the surface by conducting boundary layers. Here, a parametrized macroscale convection model will be used that utilizes thermal boundary layers at the top and bottom of the mantle [173]. The thickness δ_{upper} of the mantle's upper boundary layer is found as

$$\delta_{upper} = \frac{D_m}{2a}\left(\mathrm{Ra}_c \frac{\eta\kappa}{(T_{surf} - T_m)\alpha_V g D_m^3}\right)^{\beta_c}, \tag{2.5}$$

in terms of the mantle Rayleigh number Ra_c, mantle thickness D_m, surface temperature T_{surf}, mantle temperature T_m, Io's semi-major axis a; β_c is the convective exponent, α_V is the mantle thermal expansion factor, κ is the convection thermal diffusivity, η is the Maxwell viscosity, and g is the surface gravitational acceleration. The thickness of lower boundary layer of the mantle δ_{lower} can be related to that of the upper layer [172, 210] as:

$$\delta_{lower} = \frac{\delta_{upper}}{2}(\gamma(T_c - T_m))^{-1/3}\exp\left(\frac{-\gamma(T_c - T_m)}{6}\right), \tag{2.6}$$

with T_c the core temperature, and γ a viscosity ratio constant. The heat escaping both the core and mantle is limited by conduction through these boundary layers:

$$Q_{Conv} = 4\pi R_m^2 k_m \frac{T_m - T_{surf}}{\delta_{upper}}, \tag{2.7}$$

$$Q_{CMB} = 4\pi R_c^2 k_m \frac{T_c - T_m}{\delta_{lower}}, \tag{2.8}$$

where k_m is the mantle thermal conductivity, and R_c and R_m the outer radius of both the core and the mantle. Here, the assumption is that the core temperature is equal to that at R_c: this is appropriate for Io, where questions of an inner-outer core division are not relevant, and the core's thermal inertia is the only concern. The surface temperature of the satellite may be approximated by assuming that greybody radiation from the surface is equal to insolation plus the heating from the interior, that is

$$T_{surf} = \left(\frac{(1-A)L_*}{16\pi a_*^2 \epsilon_v \sigma_B} + \frac{Q_{Conv}}{\sigma_B}\right)^{1/4}, \tag{2.9}$$

where L_* is the stellar luminosity, a_* the stellar distance, A is the albedo, ϵ_v the emissivity, and σ_B the Stefan-Boltzmann constant. A thin/minimal atmosphere with no significant greenhouse effect has been assumed. As

[1] Equation 2.4 is valid for low eccentricities, zero inclination, and synchronous orbits [183, 208, 51].

described by Moore (2003) [161], many possible equilibrium states are possible, whereby the total radiogenic and tidal heat production rate for Io is matched by the bulk rate of convective cooling. Convective cooling rises monotonically with temperature and tidal heating as a function of temperature has one or more peak values. Tidal-convective equilibrium systems typically contain a hot-stable equilibrium (HSE) near T_{br}, the breakdown temperature[2](which is here assumed to be around 1800 K for peridotite at Io pressures [161]). A cold and unstable equilibrium typically exists well below the solidus temperature T_s. These equilibrium points are typically very stable due to the steep slope of both tidal and convective cooling curves in the onset-melting region where they often meet. The location of equilibrium points is also a strong function of orbital eccentricity. For any system, there is also a critical eccentricity, below which tidal heating is so weak that no equilibrium points exist and this is essential when studying the evolution of tidal-convective systems in time.

2.5.2 Material strength dependence on temperature and partial melting

For olivine at Io's mid-mantle pressure of ~1.5 GPa, the solidus and liquidus temperatures are 1600 K and 2000 K respectively [237], therefore the homogeneous material found in the mantle is melt. The strength and effective viscosity of the mantle will depend upon temperature and melt fraction. Viscosity is assumed to decrease with increasing temperature via an Arrhenius relationship ($\eta = Ae^{\frac{E_a}{RT}}$). The rate of decrease will become rapid once a critical melt fraction (50%) is reached, eventually becoming that of a liquid once the mantle is completely molten [162]. In addition, the strength of the mantle will decrease at this critical fraction. The strength and effective viscosity affect both the convective vigor of the mantle and the rheological response.

2.5.3 Rheological response

The imaginary part of the second order Love number, used to calculate the tidal heating within the mantle, is found via the compliance of the mantle [51]

$$-\mathrm{Im}(k_2) = -\frac{3J_U \mathrm{Im}(\bar{J})}{2[\mathrm{Im}(\bar{J})]^2 + 2[\mathrm{Re}(\bar{J}) + J_U\tilde{\mu}]^2}, \tag{2.10}$$

where $\bar{J}$ is the complex compliance, or creep function, of the mantle and depends on the rheology considered, J_U is the unrelaxed compliance, and

[2]For minerals, the breakdown temperature, or disaggregation temperature, is the point in partial melting where solid grains loose mutual contact in a growing fluid bath, above which a material rapidly takes on bulk properties more resembling a fluid.

$\tilde{\mu}$ is the effective rigidity, that is, a measure of the relative strength of the satellite to its own gravity. Equation 2.10 is derived from the definition of the static Love number $k_2 = (3/2)(1+\tilde{\mu})^{-1}$ [137]. This can be used to calculate the complex Love number $\bar{k}_2 = (3/2)(1+\tilde{\mu}J_U/\bar{J})^{-1}$. The phase angle ϵ_2, by which strain differs from applied stress can be expressed in a similar form [51]:

$$\tan(\epsilon_2) = -\frac{J\tilde{\mu}\mathrm{Im}(\bar{J})}{[\mathrm{Im}(\bar{J})]^2 + [\mathrm{Re}(\bar{J})]^2 + J\tilde{\mu}\mathrm{Re}(\bar{J})}. \tag{2.11}$$

Bierson and Nimmo (2016) [12] performed an analysis comparing Io's measured $\mathrm{Im}(k_2)$ to a predicted value usign a reduced Andrade model, where the assumptions are valid if $5\times10^{-3}\zeta^{-1/3} \ll 50$, and $5\times10^{-3}\zeta^{-1/3} \gg 1$ (ζ is the Andrade Empirical Timescale). This is satisfied, e.g., for $\zeta = 10^{-8}$, but it is strongly dependent on temperature.

2.5.4 Andrade parameters and their frequency dependence

The Andrade exponent α has been constrained between 0.1 and 0.4 [251, 68, 105] for olivine with slightly lower values for other rocky/icy materials [148, 147]. The term ζ is defined as the ratio between the Andrade and Maxwell characteristic timescales $\zeta = \tau_A/\tau_M$ [51]. The value of ζ is determined by the underlying creep mechanisms compared to a purely Maxwellian creep. Under diffusional creep, which is assumed to dominate within Io's mantle [3], $\tau_A \sim \tau_M$, thus $\zeta \sim 1$ [250][27]. Some laboratory studies on Earth materials have found small values, such as $1\times10^{-4} < \zeta < 1\times10^{-10}$ [105, 102], as well as $\zeta \sim 1$ [104]. What will be discussed here is a mantle that is subjected to a single rheology no matter its temperature or frequency. As seen, a large ζ will cause the Andrade response to reduce to that of Maxwell. The critical frequency depends upon temperature and the activation energies of the underlying mechanisms [109]. In the next sections, ω_{crit} will be taken as contant and consistent with the system under study (Io's orbital period is 1.7 days), and ζ will be taken as

$$\zeta(\omega) = \zeta_0 \exp\left(\frac{\omega_{crit}}{\omega}\right). \tag{2.12}$$

2.6 Results

2.6.1 Equilibrium results

Equilibrium states form when convective cooling is approximately equal to internal heat generation, but several equilibrium points could be possible and they can change over time due to changes in the satellite's orbit [201]. Equilibrium points consist in the crossing between convection and total heat production, both depending on temperature and partial melting.

All rheology models have the same hot-stable equilibrium before the mantle breakdown temperature ($T_{br} \approx 1800$ K). If a mantle reaches this equilibrium then it will be able to mantain high temperatures (with large melt fractions) for long time periods assuming the forcing eccentricity is not completely dissipated. The Burgers rheology produces a secondary peak to the left of the primary Maxwell peak due to its secondary material resonance. This leads to the possibility of additional equilibrium positions. This secondary peak allows a mantle to mantain a moderate temperature (with near zero melt fraction) for long time periods. A similar secondary peak occurs for the Sundberg-Cooper model, however if eccentricity is half Io's modern eccentricity, there is no crossing with convection as occurs for the Burgers curve. These results can be seen in figure 2.2.

Mathematically, there may be a point where heating and cooling meet, but in real objects with deviations from averaged behaviour this could be unimportant. The overlap depends on the relative strength of convection and tidal heating and a change in eccentricity can lead Io into or out of this quasi-equilibrium. The observed temperatures for Io's magma [114, 43] are consistent with large portions of Io's mantle being in this broad stable-equilibrium position today. This suggests that Io could have had a lower eccentricity in the recent past, or that it could be in a tidal-advective HSE point near $T_s = 1600$ K at the modern eccentricity value of 0.0041.

2.6.2 Strength and viscosity

When a mantle warms up, viscosity decreases with constant shear modulus as long as the material is solidus, and tidal heating increases. After the solidus temperature, the shear modulus starts decreasing slowly and tidal heating keeps increasing until a certain point. Afterwards, as temperature rises, the breakdown temperature is reached, the shear modulus drops fastly and tidal heating decreases. This can be seen in figure 2.3. The mass M_{sec} of the object in which tides are being generated is the most influent parameter and there is an optimal M_{sec} at which non-Maxwell features most prominently emerge. In this case, the optimal mass is $\sim 100 M_{IO}$. One of the main differences seen going from Maxwell to Sundberg-Cooper model is the expansion of high-dissipation regions, given by the inclusion of more grain scale phenomena thanks to modern laboratory results.

2.6.3 Time domain

It can be shown that the Burgers, Andrade, and Sundberg-Cooper rheologies have the greatest impact for cooler mantles and, therefore, as the object cools with time, it may pass through points where tidal heating is higher than in the Maxwell model. It is interesting to study how an Io-like moon

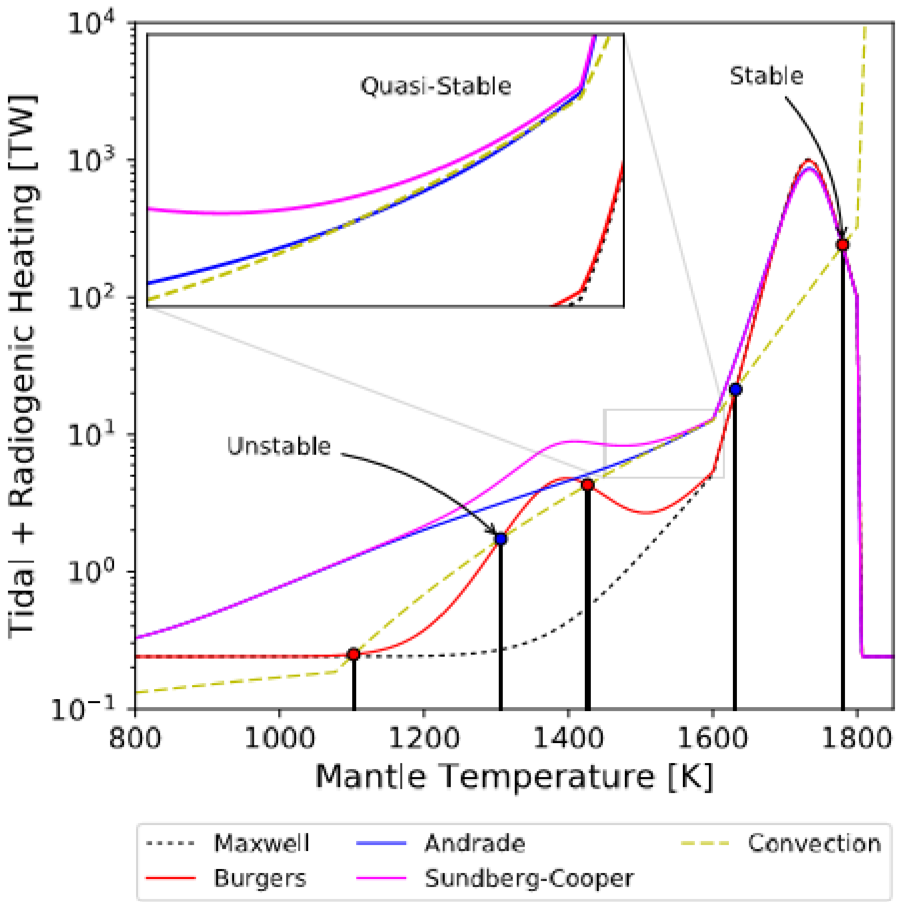

Figure 2.2: Plot of the results resumed in Section 2.6.1, using half Io's modern e. The assumed solidus and breakdown temperatures are 1600 and 1800 K, respectively. The assumed mantle shear modulus is $M_U = J_U^{-1} = 60 \times 10^9$ Pa. As seen, there is a quasi-stable region for central temperatures, and the Maxwell rheology is substantially different from the other ones for the same range of temperatures. Image taken from [193].

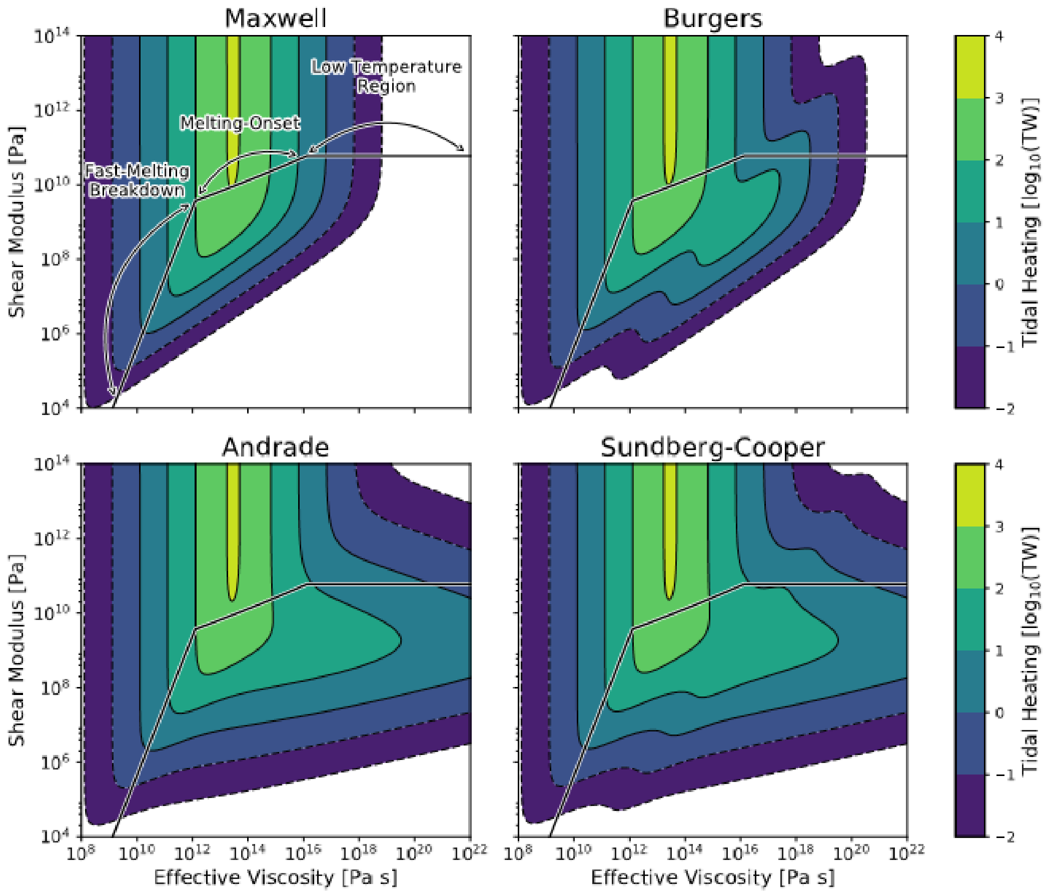

Figure 2.3: The different paths described in Section 2.6.2, represented by the black lines. As the temperature increases, the mantle moves along these lines from right to left. The modern Io's semi-major axis and half of its modern eccentricity have been used. As shown, going from the Maxwell rheology to the Sundberg-Cooper rheology increases the range of both parameters over which elevated tidal dissipation will occur. Image taken from [193].

would respond to an increase or decrease in tidal forcing. If the eccentricity is lowered from $e = 0.55e_{present}$ to $e = 0.16e_{present}$, and then increased from $e = 0$ to $e = 0.75e_{present}$, both the Andrade and Sundberg-Cooper models lose temperatures slower than the Maxwell model and warm the object faster (temperature decreases when eccentricity is lowered and increases when eccentricity rises). If the cooling lasts for too long, the Maxwell and Burgers rheologies may not respond to the upward step due to a too viscoelastically cold mantle.

In a cyclical scenario (eccentricity keeps increasing and decreasing cyclically) with high frequency, the conditions in the mantle do not vary significantly before restoration of tidal forcing. At sufficiently low frequencies, if cooling lasts long enough, tidal heating gets so low that it cannot go back to the original value even when the initial e is restored, causing the body to keep cooling. Another interesting situation is that of a sinusoidal variation in eccentricity, which is a normal situation for systems locked in mean-motion resonances (MMR's) such as Io and the other Galileian satellites. Both amplitude and period are important parameters that affect the body's thermal evolution. In particular, the term "tidal resilience" is the ability of a system to mantain tidal activity in the face of perturbations: since low-e perturbations can make a Maxwell body cold and inactive, this rheology lacks tidal resilience. On the other hand, the Andrade and Sundberg-Coope rheologies have a high tidal resilience.

From observations, it seems that Io is at (or close to) its hot stable tidal-convective equilibrium [161]. This is supported by the fact that Io is volcanically very active with high-temperature lavas [151, 114, 43]. The most credible upper limit is 1613 K [114], with an uncertainty of 50 - 100 K due to possible cooling during the adiabatic ascent or to possible heating due to viscous dissipation. This temperature is very close to 1600 K, which is thought to be the solidus temperature, with some uncertainty due to possible different composition. However, the mantle is relatively cold (1000 - 1300 K) and it is found in the temperature range from which Maxwell has difficulty escaping after a low-e excursion. This implies that, if the Maxwell model is the best at describing Io, it would be very difficult for the satellite to remain hot for more than 4 Gyr. On the other hand, if the Andrade or Sundberg-Cooper are more suitable for Io's mantle, their resilience can have kept the satellite warm and active. Therefore, applying the Andrade, or the Sundberg-Cooper, model, it is possible to understand how tidal activity on Io continued for so long despite a complex and ever-changing orbital environment.

2.6.4 Implications for the Galileian Laplace resonance

There are two theories that try to describe how long the Laplace resonance of the Jovian system has been active [184]. In the first one, the moons migrated outwards [255, 257, 257, 138, 211] under the influence of Jupiter's J_2 oblateness generating a positive $\dot{a}$. Initial differences in the migration rate may have caused the moons to convergently cross the 2:1 MMR positions so that they remained locked with a third object into a 4:2:1 pattern [166]. According to the second theory, migration may have occured inwards [23, 184, 25], due to magneto-hydrodinamic torques induced by the moons onto the primordial disk out of which they formed. After the disk is blown away, inward migration ends and outward migration starts as suggested by the first theory. During the inward migration, Ganymede may have locked Europa into a 2:1 MMR and later they captured Io into the 4:2:1 pattern seen today. The main difference between the two theories is the timing. According to the second theory, the Laplace resonance must have formed before the disk was swept away, which implies that the resonance formed rapidly after Jovian accretion. This implies that this resonance has remained stable for more than 4 Gyr and this can favour one model or the other. If Io was formed in a circular orbit, it would simply cool down with time. If this processed had lasted long enough, once the Laplace resonance formed, the Maxwell rheology would not be able to make Io hot again due to its low resilience.

Given a time τ_L after which the resonance forms, there are different possible outcomes depending on the rheology used. If $\tau_L = 10$ Myr, the mantle is still warm enough to reach its HSE ($T_m \approx 1800$ K) no matter which rheology is considered. If τ_L was much longer (e.g., 500 Myr), then the Maxwell model could not reach the HSE and the body would cool indefinitely, unlike in the Andrade or Sundberg-Cooper models. Since Io is thought to be in a hot state today [163, 228, 114], either Io's mantle has a Maxwell response and the resonance formed soon after its formation, or the mantle is better modeled by an Andrade mechanism and the resonance can have formed much later. It is also interesting to assume $\tau_L = 500$ Myr and use the forced eccentricity as a parameter. This is useful because it is possible to increase the time that passed before the formation of the resonance: Io could have existed for quite a long time without the resonance, but if the forced eccentricity is high enough it could still be able to reach the hot state seen today. In this situation, the result remains the same: the Andrade and the Sundberg-Cooper models are those that can start strong tidal heating even after a long cooling time. Again, if the Maxwell rheology is the one that best describes Io's mantle, then the Laplace resonance must have started within the first 100 Myr after the satellite's formation. Io is expected to migrate in the future: the calculations are pretty hard, because of the Laplace resonance and of the time variability of Io's internal viscosity, but this will surely affect the tidal output within Io. These considerations and the use of the Andrade rheology might also help explain the problem of Europa's warm ocean.

2.6.5 Frequency domain

In a system like that of Io and Jupiter, the tidal lag between the applied shear stress and the resultant strain depends on the frequency (and therefore on the period). The dependence varies from one rheology to another. All rheologies approach the Maxwell rheology in the low frequency limit, but only after passing outside the region where planetary tides are relevant. In the relevant tidal bands, other rheologies may differ from the Maxwell rheology by two or three orders of magnitude and by one order amongst each other. This means that the choice of rheology can overwhelm other errors. In order to understand the frequency dependence of the Andrade parameters, it is useful to examine both Andrade and Sundberg-Cooper models subjected to a frequency dependent ratio, where ζ increases exponentially below a critial frequency corresponding to $\sim$1 day^{-1}.

However, since the transition occurs in the band of Io-like periods, it is important to understand if the ratio dependence is actually important in Io conditions.

Chapter 3

Titan

The purpose of this chapter is to provide evidence that both volcanism and cryovolcanism must be present on Titan. Information taken from G. Faure and T. M. Mensing, Introduction to Planetary Science [56], M. K. Dougherty, L. W. Esposito, S. M. Krimigis, Saturn from Cassini-Huygens [46], R. M. C. Lopes et al. (2013), Cryovolcanism on Titan: New results from Cassini RADAR and VIMS [131], and L. Iess et al. (2012), The Tides of Titan [98].

3.1 Physical and orbital properties

After Ganymede, Titan is the biggest and most massive satellite in the Solar System, with a higher density than other saturnian satellites. Titan resembles Callisto in many ways, including mass, diameter, density and estimated abundance of refractory particles. Moreover, the gravitational attraction between Saturn and Titan is only 12% weaker than the attraction between Jupiter and Callisto, so probably the tidal friction caused by Saturn did not generate enough heat to cause Titan to differentiate internally into a rocky core and a mantle of water ice.

3.2 Surface

As revealed by the Huygens probe, the surface of Titan is dominated by water ice and methane, with features similar to rivers where methane flows and whose floors are very dark, since they are covered by organic material. There are also lakes that form a reservoir for the methane present in the atmosphere, where it is destroyed by solar radiation (see paragraph Atmoshpere). Even if Titan's meteorology appears to be dominated by a gas - liquid - solid methane cycle, its surface may be mostly dry, with linear dune systems, in the equatorial region. They seem to be east-west oriented, with a spacing of one or two kilometers and lengths of tens of kilometers. Their presence implies processes able to produce sand-sized particles, lack of surface fluids and wind velocities of 0.5 m/s. The large size of Titan and the high rock content suggest that enough radiogenic heat to cause water-ammonia-ice volcanic activity may be produced.

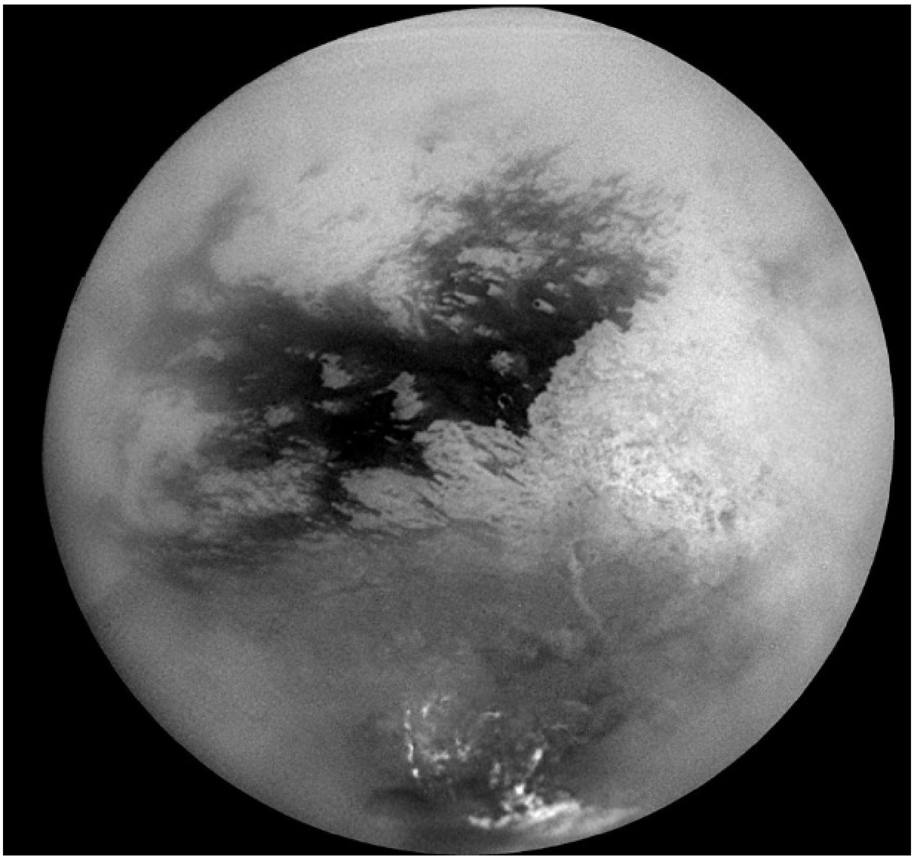

Figure 3.1: A mosaic of images of Titan's surface taken by Cassini, filtering the atmosphere.

3.3 Atmosphere

Its atmosphere is mainly composed of di-atomic nitrogen (82 to 99%) and methane (1 to 6%). Methane is particularly important, because the temperature on Titan ranges from -137 °C to -191 °C and therefore methane can be found in solid, liquid and gaseous phase (the melting point of methane is -182 °C, the boiling point is -164 °C, both at one atmosphere pressure), like water does on Earth. In the upper part of the atmosphere, solar UV photons and energetic electrons in the magnetosphere of Saturn break up molecules of nitrogen and methane, which recombine to form hydrocarbons, nitrogen compounds and oxygen compounds. In addition, the atmosphere of Titan contains molecular hydrogen which escapes its gravitational field and is continuously produced by the decomposition of methane, whereas water vapor has not been observed since it is frozen at the low temperatures of Titan. If the temperature of Titan was similar to that of Mars (-35 °C), water ice would sublimate and the resulting vapour would be dissociated in the reaction

$$CH_4 + O_2 \rightarrow CO_2 + 2H_2.$$

Hydrogen would then disappear until all of the methane would be consumed, therefore the atmosphere of Titan shows us how the primordial atmospheres of terrestrial planets might have been, because the low temperature prevented the conversion of methane into carbon dioxide. Since Titan lies in the magnetosphere of Saturn most of the time and the rotation period of Saturn is much smaller than Titan's revolution period, ionized molecules of the upper atmosphere are removed by the magnetic field of Saturn that sweeps past Titan. In this way, the methane in Titan's atmosphere would be removed in a few Myr and it must therefore be concluded that some mechanism keeps providing more methane [177].

3.4 Results from Cassini RADAR and VIMS

3.4.1 Summary of results

Thanks to recent (2013) Cassini data, it has been possible [131] to confirm or exclude the cryovolcanic origin for some features: the Ganesa region has been classified as not cyovolcanic, the same was for Tortola Facula and Winia Fluctus, the latter was discovered not to be a flow as previously thought. On the other hand, the cryovolcanic origin is more likely for Hotei Regio, the region of Sotra Patera, Mohini Fluctus and Doom and Erebor Montes, even though some features, such as Tui Regio [4], are still uncertain. Hotei Regio was supposed to be a depositional feature [159], but more recent topographic results confirmed that the previous cryovolcanic interpretation [248, 216] is more likely, since this flow is topographically higher and ticker than typical fluvial flows. Combining SAR imaging, VIMS data, and, topographic data from RADAR stereogrammetry, the Sotra Patera region has been confirmed as a cryovolcanic feature, dominated by the Doom and Erebor Montes. In this case, it has been important to combine different types of data, since deposits from highly liquid volcanic flows can be indistinguishable from features of fluvial origin, which have not been observed in this region. All the possible cryovolcanic features are located between 30°W - 150°W and 30°S - 60°N, but no particolar distribution has been found. Some interesting features are found at high latitudes [253] and near the edges of the Xanadu region [134, 133], whose boundaries could be magma conduits [191]. Therefore, it seems that Titan has experienced both volcanic and cryovolcanic activity, but some features have been eroded by the thick atmosphere and are therefore difficult to interprete.

3.4.2 Implications

The fact that cryovolcanism occured on Titan but is not the dominant surface process (e.g., [134], 2010b) has important consequences for the study of eruption style and composition. Since cryomagmas are very different from Earth-like magmas, new eruption models are needed, such as positive buoyancy through exsolution of volatiles following decompression [35, 135], explosive eruption of sprays [55], effusive eruptions due to pressurization of discrete liquid chambers [54, 212] or to an entire ocean during freezing and volume changes [139], or partial melting by tidal dissipation that forms near-surface reservoirs [157, 242]. Other theories include the inclusion of silicate material in the ice shell [36] and movement salt- or ammonia-rich ices by solid-state convection [86, 158, 30], but the cryomagma composition is an important parameter that is not constrained by observations alone. The cryovolcanic substance must surely be able to rise to the surface, to be in liquid phase on the surface and then solify, and can include both solid, liquid and gaseous compounds, in order to be less dense than the crust. The most likely solution is aqueous cryomagmas, since water ice dominates the icy satellites like Titan, with other materials such as NH_3, CO_2, CH_4, N_2, ethane, propane, acetylene [32, 117], and other hydrocarbons and organic substances. Water is a good solvent and can therefore contain several molecules, for example forming ammonium salts [110, 141].

Some surface features, such as the thick flows at Hotei Regio and Rohe Fluctus [132] can actually provide constrains on the cryolava composition and on Titan's interior. For example, the morphology and great depth of Sotra Patera is consisten with large-scale processes, such as removal of subsurface material by effusive or explosive eruptions, but the latter are likely to be suppressed by the high atmospheric pressure [135], even if Strombolian-like activity could occur due to low magma density. This implies the presence of a magma chamber, which must be due to a mantle plume rising and stalling, whose existence is possible since any cryomagma on Titan is less dense the crust. The needed buoyant force, with intracrustal intrusion, could be obtained by ammonia-water cyomagma if this was super-saturated at the source [87]. Another explanation could be the melting of crustal material, such as methane clathrates, and subsequent release of volatile compounds that would lead to exlosive volcanism [189]. It is necessary to study more deeply the properties of these materials before reaching a conclusion. Features resembling both Earth and Titan ones have been observed on Triton.

Even though they are very smaller than Titan's features, the origin may be similar and therefore the same models could possibly be applied to both satellites. The differences must be due to the different atmospheric pressure and magmatism.

Features such as the Sotra Patera region and the Hotei Regio flows are the most important evidence that cryovolcanism actually occured on Titan and played a role in its methane cycle, but if this was the dominant process, there would obviously be more features like these. Instead, as shown, it appears that effusive volcanism is far more common on Titan. The fact that no thermal signature, active plumes or surface changes have been observed, together with the fact that cryovolcanic features do not appear to be young seems to suggest that cryovolcanism is no longer going on on Titan's surface. It is expected that more and better data in the future will help to better invetigate Titan's cryovolcanic past.

3.5 Tides on Titan

Thanks to Cassini data, it has been possible [98] to reveal periodic tidal stresses on Titan, leading to a determination of its Love number k_2. Titan is deformed due to the rotation about its spin axis and to the gradient of Saturn's gravity. The response of the satellite to the external field is given by the fluid Love number k_f, whose maximum value is $3/2$ for an incompressible fluid body. For Titan, $k_f = 1.0097 \pm 0.0039$ [99], which indicates a relaxed shape, very close to hydrostatic equilibrium. The ratio between the perturbed and the perturbing potentials is the k_2 Love number, that indicated how mass responds to the potential. This second number has the same maximum as the first one, whereas a perfectly rigid body has $k_2 = 0$. It is possible to estimate the values of these numbers by measuring Titan's gravity field and its variations. Different methods [98] give the same result: for Titan, $k_2 \sim 0.6$ which indicates that this satellite is highly deformable over time scales of days. This result has been confirmed even in the case of perturbations of the dynamical model. For Titan, the value of the Love number is constrained between 0.04 (purely elastic case) and 1.0 (perfectly hydrostatic): since the calculated value is closer to that of a fluid and it is not likely that Titan has a rigidity lower than that of solid ice or rock, the conlcusion is that there must be an internal layer acting like a fluid on orbital time scales. Thus either Titan has a global low-viscosity ocean under an outer ice shell or a low-viscosity deep interior [192]. In the first case, the ice shell must be very thin so that the reaction to the stress caused by tidal forcing is that of a fluid. In such a case, the value of the shell elasticity does not significantly affect the Love number and the thickness of the ocean is also unimportant. If the deep interior is effectively rigid, the predicted k_2

ranges from 0.42 to 0.48 for a shell thickness between 100 and 0 km. For a homogeneous and entirely viscous body, the relevant viscosity is determined by a dimensionless number introduced by Darwin [42]:

$$\varepsilon = \arctan\left[\frac{19\eta\omega}{2\rho g R}\right]$$

where η is the dynamic viscosity, ω is the orbital angular velocity, ρ is the density, g is the gravitational acceleration, and R is the radius. The tidal amplitude is reduced by $\cos(\varepsilon)$ relative to the hydrostatic tide and the ratio of the imaginary to real parts of the Love number is $\tan(\varepsilon)$. For Titan, $\varepsilon \sim 0.6(\eta/10^{14})$ Pa s. The model predicts a small imaginary part of the Love number (<0.1) and satisfies the real part for a viscosity ~1 to a few 10^{13} Pa s [65], much less than the value of ice near the freezing point. The correct value for water ice depends on the stress itself and, in Titan, should be equal to that needed to carry heat out by convection. The value of k_2 could be increased by increasing the ocean's density. One way to explain the value of k_2 could be to assume a rocky core weakened by dehydration in which water can move through the cracks, but apparently this is not consistent with the expected heat flux [241]. 7. On the other hand, it is possible to assume that the global ocean contains significant amounts of sulfur that increases the density by 35%, but it has not been quantitatively proved that this sulfur can leach from the interior to the surface [60] and there is no evidence that this sulfur is actually brought to the surface [178]. A model with a simple water ocean, or ammonia-rich water, underneath a thin shell (<100 km) is consistent with all published evolution models [217], with the Huygens electric-field measurements [9], and with the estimate of the k_2 value.

Chapter 4

Enceladus

The purpose of this chapter is to provide a review of the cryovolcanic phenoma observed on Enceladus and try to explain them with a suitable model of the satellite's interior. Information taken from J. R. Spencer and F. Nimmo (2013) [226].

4.1 Introduction

Enceladus is the most cryovolcanically active satellite of our Solar System, where jets containing water vapor, other gases, and particles are ejected into space from some features found at the south pole known as ”tiger stripes”. It is very likely that Enceladus has a subsurface ocean that can be either global or local (under the south pole), probably found between an external ice shell and a silicate core. Like the other Saturn mid-sized satellites, Enceladus is large enough to be spherical, or nearly, has a relatively low density, has a very high albedo and its surface is mainly composed of water ice but, unlike the other satellites, is not dominated by craters, indicating that its surface is constantly being renewed. Enceladus is in a 2:1 resonance with Dione and this keeps it active through tidal heating. Thanks to several Cassini flybys, it has been possible to confirm that Enceladus' plumes are very likely to be the source of Saturn's E-ring. In general, Cassini data have significantly improved the understanding of how cryovolcanic activity works on Enceladus.

4.2 Observations

4.2.1 Density, gravity, and shape

Enceladus has a bulk density of 1.609 ± 5 kg m^{-3} [240], which suggests a 60:40 rock:ice mixture by mass [207]. It has been suggested [62] that the resonance with Dione could force rotational librations on Enceladus,

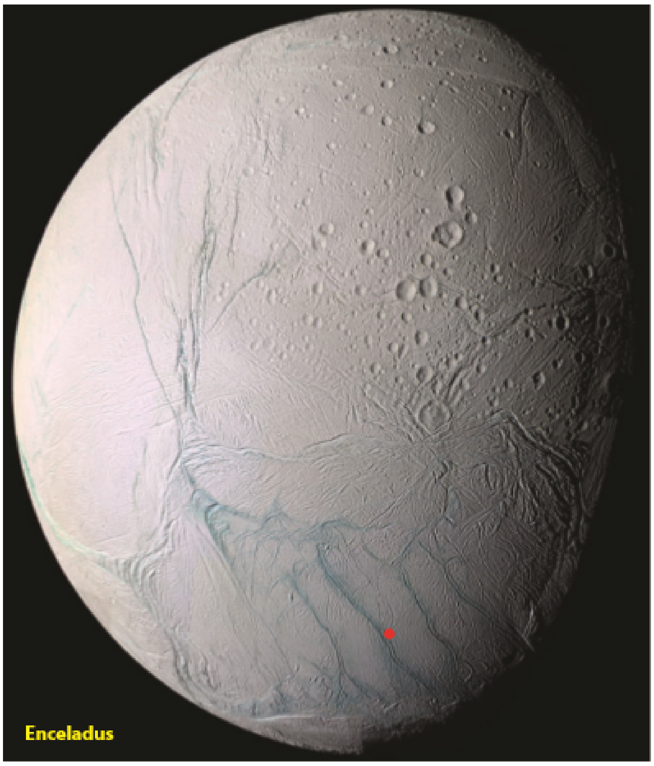

Figure 4.1: Global view of Enceladus obtained by the Cassini spacecraft, with an example of old and cratered terrain on the right and younger terrain on the left. The red dot indicates the south pole, and the four parallel bluish fractures are the famous ”tiger stripes” that appear blue because they are rich in coarse-grained water ice, which absorbs the near-infrared light used to take this false-color image. Image taken from [226].

implying that there must be a certain degree of mass concentration toward the center. However, these librations have such a low amplitude that are not significant in terms of tidal heating. The surface appears bumpy, with depressions and bulges, at 100-km-scale wavelengths but is smooth at 10-km wavelength.

4.2.2 Global geology

Enceladus' surface geology is very diverse with great simmetry [37] about its rotation axis and the direction of Saturn (which is fixed, due to its synchronous rotation). There is a region that extends from the Saturn-facing side to the opposite side passing over the north pole, which is thought to be the oldest part of Enceladus' surface, due to its high crater density, with an age of 1 to 4 Gyr [118]. However, these craters have been modified by a combination of geological and cryovolcanic processes, including pervasive tectonic fracturing, viscous relaxation, and burial by ejecta from the plumes. On both hemispheres, the central regions appear to be very young, from 2 Gyr to 10 Myr, with a series of features that indicate tectonic activity and motion, given by extensional and compressional stresses. These structures are symmetrical about the apex and antapex of motion [37], but the crater densities decrease from north to south, indicating that the southernmost regions are younger [118]. Several studies analyzed small-scale topographic features to determine the heat fluxes in the past [63, 13, 14]: equatorial rifts suggest a heat flux of 200-270 mW m^{-2}, equatorial ridges suggest a heat flux of 110-220 mW m^{-2}, and relaxed craters suggest an excess in heat flux of 150 mW m^{-2}. These estimates are similar to the heat emitted today at the south pole, suggesting that geological activity was the same when, or after, these features formed.

4.2.3 The active South Polar Terrain (SPT)

The South Polar Terrain (SPT) is a region found almost exactly at the south pole where the present-day activity is centered [186]. This region is, as suggested by the crater density, younger than a few million years [186] and is bounded at about 50°S by south-facing scarps and rugged marginal arcs. At the center of the SPT there are the famous four tiger stripes (Damascus, Baghdad, Cairo, Alexandria) where most of the activity is focused. These stripes are parallel fractures about 130 km long and spaced 35 km apart. The margins raised by the tiger stripes surround a central depression which is 2 km wide and 0.5 km deep and is the source of both thermal emission [227, 221] and the plume jets [230, 185]. Along the tiger stripes, the temperature has been found to be at least 180 K [221, 222] and the total endogenic power radiated is 15.8 ± 3.1 GW [94], as shown by Cassini measurement of the infrared emission. The uncertainty could be larger, since it is difficult to account for the thermal emissione due to absorbed solar radiation.

4.2.4 Plume structure and composition

Each tiger stripe ejects a plume and they all merg to form a single larger plume at altitude [230]. The gas plume mostly consists of water vapor, with about 5% CO_2, 1% CH_4, 1% NH_3, and traces of other hydrocarbons and organic molecules [77, 247, 246]. The plume particles are mainly water ice particles, with about 1% salt, of which most is NaCl [188]. The typical radius is a few micrometers and presumably half of the mass is given by particles with radii larger than 3 μm [100]. The particles can have a wide range of speeds and about 10% of them is fast enough to overcome escape velocity (240 m s^{-1}) [100]. The gas is surely faster than most of the particles [204], with the best estimate around 450 m s^{-1}, with the fastest gas molecules reaching 1 km s^{-1}. It has been estimated that about 200 kg of gas [77] and

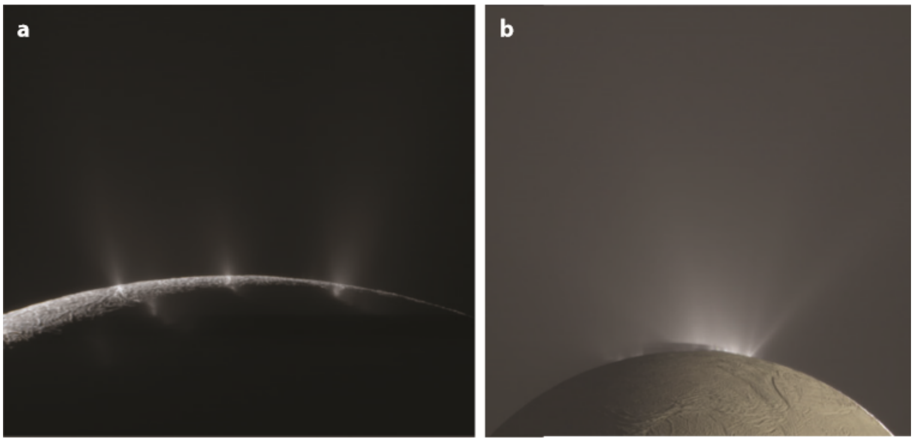

Figure 4.2: The plumes emitted by the tiger stripes of Enceladus. Image taken from [226].

50 kg of dust [100] are ejected every second, with the difference that most of the gas can escape Enceladus gravity field, while only about 10% of the dust can [88, 188]. It is possible that the near-infrared brightness of the plumes is correlated with Enceladus' position in its orbit, implying that the activity depends on tidal flexing [66].

4.2.5 Surface structure and composition

The surface mostly consists of water ice [167] with an extremely high albedo ($\sim 80\%$) [93] given by plume particles that fall back on the surface [113], as proven by the agreement between the predicted spatial distribution of plume fallout [113] and surface color patterns revealed by Cassini [202]. Infrared spectroscopy [106] and 1-μm imaging [186] reveal that the grains found closer to the tiger stripes are larger. The surface also presents CO_2 [16], H_2O_2 or light organics [16, 168], and possibly NH_3 [52], consistent with the plume composition, apart from H_2O_2 which could be produced by oxidation of H_2O. On the other hand, it is quite hard to see the salts due to their weak reflectance spectra. The temperature difference between day and night is about 30 K [93], suggesting a low surface thermal conductivity quite similar to that of other icy Saturnian satellites, due to an unconsolidated surface given by the layer of plume particles that have fallen back on the satellite.

4.2.6 Influence on the Saturn system

Today, it is definitely known that Enceladus provides the material that forms Saturn E-ring, through the plumes ejected from the south pole [113]. The vast majority of the particles in the E-ring are salt-poor, because these are the ones that have smaller masses and can more easily escape Enceladus' gravitational field. The actual importance of these particles is difficult to overestimate, since the brightness of the other mid-sized satellites decreases with increasing distance from Enceladus, implying that the plumes material can reach other satellites and affect their surfaces [245]. Sputtering quickly destroys most of the E-ring particles on timescales of decades [108, 100], but the plumes can evidently provide the same amount of material, in particular ejected neutral OH, H_2O, and O [53, 85, 209] form a torus affecting Saturn's magnetosphere more than similar species do in Jupiter's magnetosphere. What's more, Enceladus interacts with Saturn's magnetosphere also by ejecting negatively charged dust [164] that drives electrical currents along magnetic fields lines, giving rise to an ultraviolet auroral emission near Saturn's poles [190]. Water contained in Enceladus' plumes could also be an important source of oxygen for the atmospheres of Titan and Saturn itself [26].

4.3 Origin and interior

4.3.1 Bulk structure

The high heat output suggests that Enceladus should be completely differentiated, but this has not been definitely proven. Given the observed bulk density, the interior should be divided in a metal-silicate core with a radius of 150-170 km, and an ice/water layer about 80-100 km thick [207] that must have come in contact with silicates [262], in order to explain the observed Na in the erupted ice particles [188]. The interior is heated by tides and radiogenic decay: the former is negligible in the core due to the high silicate rigidity and viscosity [194] and is higher in the ice shell, especially if it is decoupled from the silicate core thanks to liquid water, while the latter is today thought to be able to generate only 0.3 GW.

The observed depression at the south pole can presumably be explained by assuming a local liquid sea underneath [31]. Since it is difficult to justify the presence of a global liquid ocean over geological timescales, it is reasonable to assume that it contains significant amounts of ammonia that acts as antifreeze [92] and delays complete freezing. In fact, as previously said, the plumes contain about 1% NH_3 [247]. On the other hand, tidal heating could be focused at the south polar region so that water is found in liquid phase only here and it is possible to find a solution that allows a regional sea and explains the observed heat output (e.g., [242]). This possible internal structure is shown is figure 4.3

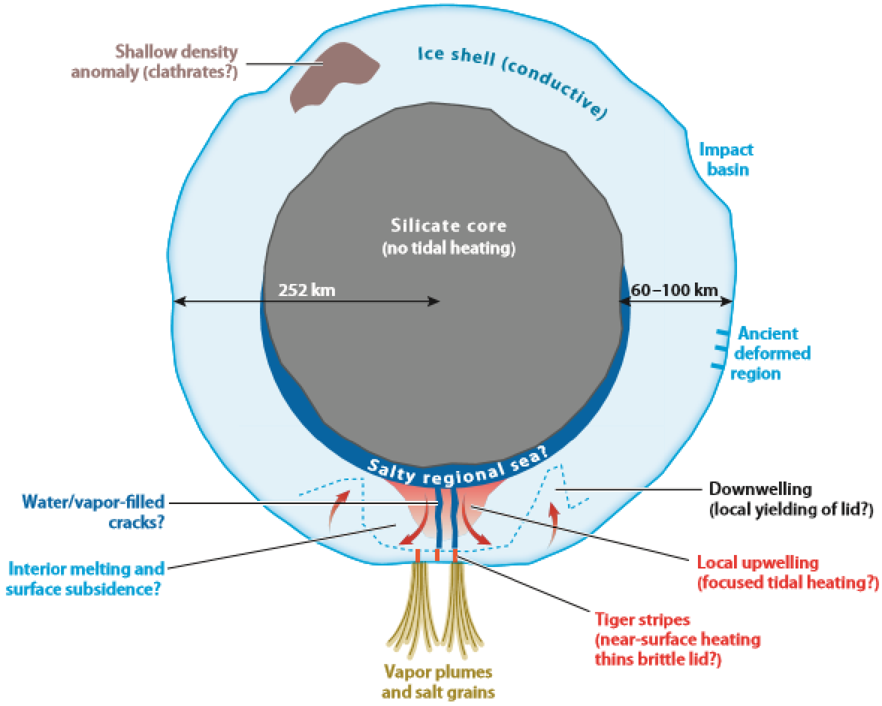

Figure 4.3: Enceladus' possible internal structure. Image taken from [226].

4.3.2 Ice shell convection and density variations

On Enceladus, ice convection is very unlikely: the gravity is low and the ice shell is thin, making convection marginal an dependent on uncertain parameters such as grain size [6], moreover convection on a global scale would be too dissipative and therefore inconsistent with long-term orbital evolution [260]. However, if solid-state convection was localized at the south pole and the near-surface ice was weak, it would be possible to explain the heat flux and the young age of the surface in this way [5, 76, 176]. If the heat transport was confined to the tiger stripes alone, it could occur via conduction (close to the surface) and advection (of either liquid water or vapor) at greater depths. Thermal convection alone is not enought (e.g., [195]) to explain the observed 1-km amplitude of global long-wavelength topography [203]. The explanation could be given by lateral shell thickness variations or lateral density variations: the latter are more likely because they can persist indefinitely, while the former will be rapidly removed by viscous flow [231]. The theory of the lateral density variations could also explain the fact that the hot spot is found at the pole [170]: convection-induced melting and drainage can produce a low-density region (e.g., [22, 219]), as well as destabilization of denser clathrates (e.g., [116]), which then reorients to its rotationally stable location at the pole. However, this is in contrast with the fact that older geological terrains are symmetrical about the currents spin axis and Saturn direction.

4.3.3 Heat source

Since no other mechanism is present, tidal heating must be the heat source within Enceladus, but the magnitude and time history, and location and nature of the dissipation are not clear. It has been suggested that tidal heating may occur in the ocean [244], but the required obliquities are definitely too high [29]. The dissipation could occur within the ice shell, either in a more distributed way (e.g., [21]) or due to frictional heating on individual fault segments [171]. Since a great deformation is needed to explain the high heat flux, the presence of a regional sea is very likely [171, 242] in order to decouple the ice shell from the silicate core, and the heat could be generated directly underneath the tiger stripes or at greater depths and then be advected to the surface. An explanation is needed for the fact that only one pole of Enceladus is active: tidal dissipation is potentially self-sustaining in a localized region thanks to a feedback mechanism (e.g., [157]), but still an initial perturbation, such as an impact, is needed. On the other hand, the geometry of the core could somehow favor geological activity at the pole [153].

4.3.4 Tidal heating and orbital evolution

The rate of tidal heat production for a synchronous body is calculated as (e.g., [166]):

$$\dot{E} = \frac{21}{2}\frac{k_2}{Q}\frac{(nR)^5}{G}e^2 = 15\text{GW}\left(\frac{k_2/Q}{0.01}\right)\left(\frac{e}{0.0047}\right)^2, \tag{4.1}$$

where$n$ is the mean orbital motion ($5.3 \times 10^{-5} s^{-1}$), R is the satellite radius (252 km), G is the gravitational constant, e is the satellite eccentricity (0.0047), k_2 is the tidal Love number, and Q is the dimensionless dissipation factor. If k_2/Q is very high, the body is very deformable: this term and eccentricity are the most influential in tidal heating. Normally, dissipation damps eccentricity, but in this case the 2:1 orbital resonance with Dione counteracts the damping [155]. Therefore, if Enceladus' eccentricity remains constant, heat production is inversely proportional to Saturn's Q and does not longer depend on Enceladus' k_2/Q [154], in addition the eccentricity adjusts itself to produce the equilibrium heating rate, depending on the value of Enceladus' k_2/Q. Today, it is assumed that $Q_{Saturn} \geq 18000$ (averaged over time), which implies a heat production within Enceladus of 1.1 GW [154], much smaller than the observed value.

Four main possibilities have been proposed to solve this problem. First, it could be that $Q_{Saturn} \ll 18000$, as suggested by Lainey et al. (2012) [123], but there are several problems: the analysis of Lainey et al. (2012) also shows an inward motion of Mimas hard to explain, moreover a smaller Q would imply different locations of the mid-sized satellites, unless they are much younger than the Solar System (cf. [28]). Second, it may be that Enceladus is actually producing 1.1 GW, but this is only released periodically [176]. Assuming a periodicity of about 100 Myr, it is possible to create a model that predicts the 200 mW m^{-2} observed when heat is released, moreover the model is compatible with the situation, supposed before, that heat is advected from a subsurface ocean via water-filled cracks. Third, Enceladus may be producing heat periodically (e.g., [175]; but cf. [156]). It is possible that Enceladus spends 10% of the time in a warm and dissipative state, during which eccentricity decreases as observed today, while during the remaining time it is cold and nondissipative, with increasing eccentricity, so that the time-averaged heat production is 1.1 GW. Given the strong feedback among heat production, temperature, and ice viscosity, this heating can naturally arise, even in a restricted area (e.g., [22]). Fourth, it is possible that the heat flow has been overestimated: if it were actually lower, Enceladus would be allowed to spend more time in the present state and the probability of observing it during the active state increases. However, this is very unlikely since the majority of the thermal emission is undoubtedly associated with the tiger stripes, therefore it is unlikely that more than 14 GW have wrongly been associated to Enceladus' heat flux.

The observed $k_2/Q = 0.01$ of Enceladus seems to suggest that possibilities two and three are correct, since they assume that Enceladus is active 10% of the time. However, there are two problems: first of all, the time-averaged value of k_2/Q must be less than 0.0008 due to its escape from the resonance with Dione, moreover it is unlikely that we are actually observing Enceladus exactly during the active time.

4.3.5 Long-term geological and ocean evolution

The geological evidence seems to support the idea that Enceladus becomes active periodically, after spending a long time in a cold state: the surface seems to show that different regions experienced tectonic activity and heat fluxes at different times. If the 1.1 GW are distributed globally, this is not enough to sustain a global liquid ocean over geological timescales [194], but if the heat flux is focused around the south pole, this is enought to sustain a regional sea indefinitely [22, 242]. In this way, the local sea can have existed for as long as the resonance with Dione did, and the same could have happened in other regions during different times, explaining the older activity observed all over the surface.

4.3.6 Formation

The formation of the satellites is a crucial moment, because it determines the initial thermal state and the rock:ice ratio, which are important for the subsequent evolution (e.g., [165]). Since Enceladus has a small mass, it did not receive much energy during the formation, therefore the heat needed for differentiation depends on the ratio between the formation timescale and the decay timescale of ^{26}Al (half-life of 0.7 Myr), the mass fraction of the silicates containing ^{26}Al and any other radiogenic heat sources. It is possible that Enceladus accreted while ^{26}Al was still decaying if the estimate of a formation timescale of 0.1-1 Myr [24, 165, 174] is correct. Unlike Mimas, Enceladus' eccentricity may have been increased at some point due to some resonance, leading to a runaway effect that started strong tidal heating (e.g., [22]). The difference between the two satellites could have developed during formation: Mimas has a lower rock:ice ratio and therefore should have experienced less ^{26}Al heating but, on the other hand, since Mimas is closer to Saturn, it should have formed more rapidly and should have experienced more ^{26}Al decay.

4.4 Understanding south polar activity

4.4.1 Tectonics

Within the SPT, there could be thermal expansion [64] going on due to the heat coming from the tiger stripes, that would explain the equatorward motion of material observed at the edge of the SPT. This mechanism could explain both the young age of the SPT and the high regional heat fluxes [5]. The morphology observed between the tiger stripes may indicate that mobile-lid convection is going on, with a lid thickness of $<$400 m [7].

It has been proposed [182] that some features found in the SPT show progression in orientation with age. In particular, the authors suggest that traces of ancient tiger stripes with a different orientation than the modern ones can be seen, leading to the conclusion that nonsynchronous rotation has occured in the past. However, these features are not clearly distinguishable and a nonsynchronous rotation is mostly inconsistent with the observed simmetry about the present-day rotation axis. The reorientation theory suggests the presence of east-west thrust faults, which may actually be present [182], and extentional stresses toward the equator, which may in fact be consistent with the observed young north-trending fracture sets. On the other hand, this theory is inconsistent with the distribution of impact craters [118]. The orientation of today's tiger stripes is the one that maximizes the normal extentional tidal stresses [171], so they probably formed as tension cracks.

4.4.2 Plume source and mechanics

Water surely plays an extremely important role in the production of Enceladus' plumes. In order to explain the large grain mass, it has been proposed that the mechanism is the violent boiling of the liquid source directly into space [186], but it is difficult to provide heat to a liquid in space without freezing of the liquid itself [187]. What's more, it has later been observed that these grains are rich in sodium salts [187, 188], while the vapor is sodium poor [206]: therefore these two componenst have two different sources. On the other hand, the ice grains have a salty composition, as expected for water in equilibrium with a silicate core [262], implying that the source consists of liquid water. The most reasonable hypothesis, in order to explain the salty composition, is that flash freezing of salty liquid water is going on at the source. A possible explanation has been provided by Postberg et al. (2009) [187]: they suggest that water may be evaporating more slowly, over a larger area, into pressurized chambers and then reach the surface through narrow fractures. In this theory, the bursting of gas bubbles at the water surface has been proposed as alternative explanation for the salty composition to the flash freezing. This is reasonable, since gases such as CO_2 and CH_4 are present in greater abundances than expected by their solubility in water [247]. Therefore, these gases must come from a nonaqueous source, unless most of the water releases its gases and is then recycled [146].

The thermal signature is consistent with conductive heating of the surface by fractures with temperatures above 200 K [1]. A possible way in which heat may be transfered is by advection of plume gases up the fractures [171, 227] and then by condensation of H_2O vapor on the fracture walls [101], but this would close the cracks at a rate of up to 1 m year^{-1}, limiting the lifetime of each fracture. Heat production is another important matter: it could be due to shear heating by tides at shallow depth [171], but this is correlated to the efficiency of heat transport: heating reduces ice viscosity, which itself reduces heating and therefore heat must be quickly transfered. Heat may also be brought to the surface thanks to water ascending through cracks [146, 185]: gas bubbles might reduce its density so that it can rise buoyantly through the crust [35, 146], where the fractures are kept open by water pressure [35]. There is evidence [66] that plume activity is correlated to the change in diurnal stresses [96]. Gas particles can then reach supersonic speeds when once they get into the vacuum space, as observed [204], while larger particles are slowed down by collisions with the conduit walls.

Chapter 5

Charon

5.1 Introduction

Charon is very representative of the smaller Kuiper Belt Objects (KBOs), with a radius smaller than 750 km. These bodies show absorption features of amorphous or crystalline water ice, and Charon also shows a feature (2.21 μm) that presumably is due to ammonia hydrates. Since the temperature here is too low to account for the presence of crystalline water ice, which should be amorphized by cosmic rays, a mechanism of surface renewal on short timescales must be present. This mechanism must also explain the presence of ammonia hydrates and must be valid for other KBOs, such as Quaoar. It turns out that cryovolcanism is the most likely mechanism.

5.2 Comparison between observations and models

In order to understand the surface composition, it is necessary to compare observed reflection spectra with the spectra that are expected to be reflected by various combination of materials and particle sizes. This has been done by J. C. Cook et al. (2007) [33] using the spectra predicted using Hapke's theory of spectral reflectance [81]. The materials used in this analysis include crystalline water ice (I_h), a dark neutral absorber (dna), and an ammonia hydrate ice (I_{NH}) with other components. The models generates spectra using laboratory spectra of these materials for inputs: it has been considered that crystalline water ice spectrum has a strong dependence on temperature [71], while amorphous water ice spectra are less temperature-dependent [200, 205], and the spectra of ammonia hydrates were taken from Brown et al. (1988) [17], considering all possible hydration states, that is ammonia dihydrate (ADH, $NH_3{\cdot}2H_2O$), ammonia monohydrate (AMH, $NH_3{\cdot}H_2O$), ammonia hemihydrate (AHH, $NH_3{\cdot}1/2H_2O$), or water and ammonia Using descriptions made by Bertie and Shehata (1984) [11], the hydration state is probably ADH, with optical constants calculated by Bauer et al. (2002) [8]

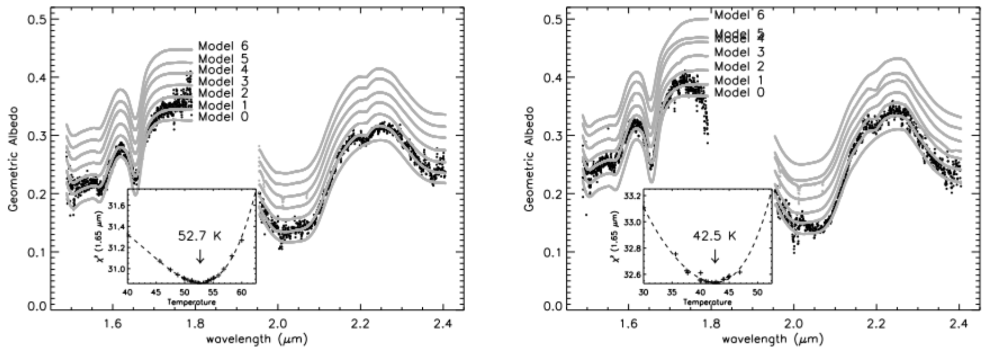

Figure 5.1: Observed spectra (black dots) and fits (lines) to the sub-Pluto (left) and to the anti-Pluto (right) hemispheres of Charon. The insets show χ^2 as a function of temperature for 1.60 - 1.70 μm only. The t for model 1 is centered on the observations. All other ts are displaced by increments of 0.02. Image taken from [33].

and Cruikshank et al. (2005) [39], but the 2.21 μm feature shifts to shorter wavelengths when the hydration state changes and no optical constants were calculated for this situation. The dna has been taken from Buie and Grundy (2000) [19]. Observations prove that small-grained I_h does not fit in the continuum but does with the 1.6 and 2.0 μ features, whereas large-grained ice does the opposite, but even mixing the two did not fit the continuum properly. Since the compounds that have been tried did not behave like the dna observed, the needed features for a ad hoc material have been directly derived from the observed spectra. Different models have been tried, using amorphous carbon [199], methane ice [72], carbon dioxide ice [78, 79], or ammonia ice [142], but the optical constants for CO_2 and NH_3 were only avaiable at specific temperatures, while a reasonable interpolation of the spectra was possible for methane and amorphous water ice.

5.3 Results

Using seven different models, it is clear that I_h dominates the surface and it is even possible to determine its temperature. The 2.21 μm feature can be due to ammonia [48], its hydrates, or HCN [19, 15, 48], but the latter must be excluded since its other aborption features are not present [143], unless the abundance is very low [143]. The ammonia feature at 2.01 μm is very different from the one observed on Charon, and the one at 2.24 μ has not been observed, therefore ammonia can only be present in very low abundances and with very large grains. The models with ammonia hydrates have a better χ^2: the anti-Pluto hemisphere has a spectrum matched by a feature of ADH [11], while the other hemisphere has this feature shifted as expected for AHH [10]. Therefore, the 2.21 μm feature belongs to I_{NH}, with different hydration states on the two hemispheres. Fitting other ices lead to the conclusion that CO_2 could have an abundance up to 30% and a grain size up to 100 μm, while methane must have an abundance lower than 2% and a grain size greater than 100 μm. However, the models do not fit the 1.65 and the 2.1 μm features, and do not match the decrease in geometric albedo for $\lambda > 1.75$ μm. The conclusion is that another element is present and that the best fit is obtained when ADH is used.

5.4 Discussion

The comparison between observations and models confirms that Charont's surface is dominated by water ice and also contains ammonia hydrates. What's more, these hydrates could exist in different hydration states on the two hemispheres. In the following part, the fact that the two hemispheres may have different temperatures will be considered. In addition, the presence of crystalline water ice implies that there is a continuous renewal process on a geologically short timescale. It will be shown that the ammonia hydrates which are present are not primordial and several possible renewal mechanisms will be analyzed.

5.4.1 Temperature estimates

Spectra of H_2O ice in the near-infrared with temperatures 20 K $\leq$ T $\leq$ 270 K show [71] show that the spectrum changes with temperature. In this spectral region, the 1.65 μm feature is the most sensitive to temperature and has been used to determine the temperature of several icy bodies of the Solar System [70], therefore it can be used for Charon as well. A model with I_h and dna has been used to minimize χ^2 with respect to temperature. The estimated temperature is 42.5 K for the sub-Pluto hemisphere and 52.7 K for the anti-Pluto hemisphere. A Gaussian fit gives basically the same result as more complicated fits, with an uncertainty of 5-10 K for each temperature. Not only the two hemispheres have different temperatures, but their spectra also have minima at different wavelengths. It seems unlikely than one whole hemisphere is 10 degrees warmer than the other one, so these temperatures should be attributed to different patches of ice. The local, instantaneous blackody temperature of ice is given as:

$$T = 70.9(1-a)^{1/4}(cos\theta)^{1/4}\text{K} \tag{5.1}$$

where a is the visual albedo and θ is the altitude of the Sun in the sky. Maps show [20] that Charont has some patches of ice with a very high albedo, $a \approx 0.7 - 0.9$. Therefore, in the case $\theta = 0$, the typical temperatures would range from 39.9 K to 52.5 K. This proves that the temperatures derived from the 1.65 μm are completely consistent with those derived theoretically.

5.4.2 Presence of crystalline water ice

The presence of crystalline water ice is definitely normal on Charont, since it has been observed on several other satellites [70] and KBOs [107]. However, it is not known whether the ice is purely crystalline or a mixture of crystalline and amorpohus, sinche the first one would dominate the spectra [70]. However, the presence of crystalline water ice on Charont is surprising, because it cannot be created in these outer regions of the Solar System without heating. Radiation tends to destroy the bonds that keep the water ice in an ordered structure and, at these temperature, ice cannot reassemble itself into crystalline form. First of all, it is necessary to calculate the rate at which water ice is amorphized by radiation. These rates have been quantified for radiation in the form of energetic ions (i.e., cosmic rays) [89, 160, 232, 144] and in the form of UV photons [120, 125, 126]. The ability of both types of radiation to amorphize ice scale with the energy deposited in the ice is the dose. The $1/e$ dose necessary to amorphize ice by UV irradiation, $k = 2 - 3$ eV per molecule at ≈ 50 K, is nearly identical to the doses required for amorphization by proton irradiation and He^+ irradiation [160, 232, 125]. The dose of cosmic rays received by the KBOs has been calculated by Cooper et al. (2003) [34] and it has been found that the time for ice at depth d to accumulate a dose of 100 eV per molecule increases linearly with d. At the maximum depths probed by H and K measurements (350 μm), the timescale to accumulate 100 eV per molecule is about 10^8 years. Therefore, the time to accumulate 3 eV per molecule is 30 times lower. Averaging from the maximum depth to the surface, the time is halved. In the end, the $1/e$ amorphization time due to cosmic rays is about 1.5 Myr. UV and visible solar photons are even more effective: UV photons between 100 and 180 nm can only penetrate ice to depths of 1 mm, but UV/visible photons from 180 to 620 nm can reach depths of about 1 m. The dose D of solar UV radiation received by ice at different depths x over one Pluto orbit is:

$$D(x) = R_\odot^2 \int^{1Pyr} \int_{\lambda_1}^{\lambda_2} \mathcal{F}_\odot (1 - a_\lambda) \frac{\alpha e^{-\alpha x / sin(h(t))}}{r(t)^2 n_{H_2O}} d\lambda dt \qquad (5.2)$$

where $R_\odot$ is the solar radius, r is the heliocentric distance, $\mathcal{F}_\odot$ is the solar flux at the Sun's surface from 100 to 620 nm [73], $a = a_{UV} \approx 0.25$ for $\lambda < 350$ nm and $a = a_{vis} \approx 0.38$ for $\lambda \geq 350$ nm [122, 44] are the albedos, α is the absorption coefficient per molecule [249], and $n_{H_2O} = 3 \times 10^{22}$ cm^{-3} is the number density of H_2O molecules in the ice. Calculations show that the latitude does not efficiently affect the dose received.

The average crystalline fraction down to depth d is given by:

$$\langle f_c \rangle = \frac{1}{d}\int_0^d e^{-kND(x)}dx \tag{5.3}$$

where N is the number of Pluto orbits completed. By setting α_{IR} to the average absorption coefficient between 1.4 and 2.5 μm, it is found that $d \approx 350\mu$m. The amorphization timescale is defined as the time needed to reduce the crystalline fraction to $1/e$. The typical value for this timescale is $(3-5)\times 10^4$ yr, much shorter than the age of Charont and than the timescale on which ice is thermally annealed at 50 K, that is $t \approx 10^{26}$ yr. Since UV and visible photons can penetrate up to about 1 m, the ice between 0.1 mm and 1 m is amorphized in a few million years. Even at much greater depths (100 m), ice could easily be amorphized on a geological timescale (100 Myr), but since the ice on Charont is predominantly crystalline ($\gg 90\%$) it must be concluded that something is replenishing crystalline water ice on a timescale shorter than 10^5 yr.

5.4.3 Presence and dichotomy of ammonia hydrates

Since ammonia hydrates are common among icy satellites, outer planets, and KBOs [17, 8, 107, 15], ancient comets have been analyzed [112], finding an abundance ratio of $NH_3/H_2O \approx 0.5\%$, which is a lower limit since ammonia is more volatile than water. Analysis of the icy satellites [58] and of Titan's atmosphere suggested ratios between 5 and 20%, while IR observations [236, 41] of massive protostars showed ratios between 5 and 7%, and chemical equilibrium models with Solar System abundances predict ratios of 15% - 20% [129, 44, 127]. Ion bombardment from Pluto has been proposed as source of NH_3 [48], but the high energies would remove the ammonia [233] and this cannot be applied to other KBOs where ammonia has been detected. Since ammonia hydrates should be destroyed by radiation in under 20 Myr [34], some sort of surface renewal mechanism must be present, and the fact that the equilibrium condensate from solar nebula gas is ADH [129], while on Charon AHH is present, implies the presence of chemical processes.

5.4.4 Mechanisms for surface renewal

The presence of I_h demands some heating or surface renewal process, since Charon's eccentricity is too low to cause tidal heating. For example, it could simply be present in the interior and be periodically brought up by micrometeorite impacts or by solid-state convection. Otherwise, water vapour could slowly deposit and freeze onto the surface as crystalline water ice. However, differently from Pluto, this vapour does not come from a global atmosphere: data show [74] that if all the avaiable vapour were frozen as frost, it would form a layer less thick than 120 μm, so even less thick than the depths probed by H and K spectra. So, vapour could temporarily be formed by impacts. Another theory suggests that amorphous ice could be heated to a warm temperature long enought to anneal to crystalline form (e.g., [47]). The time needed for this increases exponentially with lower temperatures according to an Arrhenius relation [121]. This timescale exceedes the age of the Solar System unless $T \geq 77$ K. On Charon, these temperatures cannot be found and therefore an intense heating is required to make this theory plausible. Finally, crystalline water ice could come from the solidification of liquid water, brought to the surface from deeper and warmer layers of Charon (cryovolcanism). Each of these processes could actually contribute to the presence of crystalline water ice on Charon's surface, where it is then amorphized.

Impacts

Considering that about 20% of Charon's surface has been struck by impactors large than 1 m (the lack of an atmosphere allows every meteorite to reach the surface) in the last 3.5 Gyr [49], the fraction of surface struck in one amorphization timescale is $(0.20)(10^5 \text{ yr})/(3.5 \text{ Gyr}) \sim 6 \times 10^{-6}$, and therefore this process cannot uncover crytalline water ice. Considerations about the diameter of the impactors [259] show that considering meteorites smaller than 1 m does not significantly change the result.

The mass flux of dust particles is $\approx 2.4 \times 10^{-17}$ g cm^{-2} s^{-1} [95, 239], so if each one has the mass of the smallest ones detected by Pioneer 10, 8.3×10^{-10} g, the number density is $\approx 3 \times 10^{-8}$cm^{-2}yr^{-1}. If each one makes a crater with a diameter of 100 μm, over 3.5 Gyr the surface cratered by micrometeorites is about 1% of the total surface and therefore this mechanism cannot explain the observations.

The total kinetic energy flux on Charon is therefore 2.6×10^{-7} erg cm^{-2}s^{-1}, thus a layer as thick as the one probed by H and K observations can be vaporized and refrozen on timescales of about 13.5 Myr, much longer than the 0.05 Myr needed by UV/visible photons to amorphize the ice. Instead, if the energy was used to heat the ice above 200 K, the annealed mass of ice would be 10 times the impactor mass, independent on the impactor mass itself. This is obtained assuming that none of the heat is lost to vaporitazion or mechanical work, assuming the heat capacity calculated by Shulman (2004) [213] ($C_p \approx 1.0 \times 10^7$ erg g^{-1} K^{-1}), making reasonable assumptions about the values of thermal diffusivity ($K = 2 \times 10^{-5}$ cm^2 s^{-1}), thermal conductivity ($\kappa \approx 100$ erg cm^{-1} s^{-1} K^{-1}), ice density ($\rho = 0.5$ g cm^{-3}), time of crystallization at 200 K ($t_{crystal} = 9.54 \times 10^{-14} e^{5370 \text{ K}/T}$ s), impactor mass ($m_p = 8 \times 10^{-10}$ g), and using observed values of the thermal inertia ($\Gamma = (\rho C_p \kappa)^{1/2} \approx (3-7) \times 10^4$ erg cm^{-2} s$^{-1/2}$ K^{-1}) [220, 225, 229].

Therefore, the mass of ice annealed is about 10 times the total mass flux of micrometeorites and therefore the $1/e$ annealing timescale results 3.1 Myr or more, considering that heat is actually lost to mechanical work and vaporitazion. Therefore, since the annealing timescale given by micrometeorites is at least 4.5 Myr, and the amorphization by UV/visibile photon has a timescale of 0.05 Myr, the conclusion is that this mechanism cannot explain the presence of more than 90% of crystalline water ice on Charon's surface.

Solid-state greenhouse

This effect is due to the fact that ice is transparent to visible radiation but opaque to infrared radiation, so ice at depth is heated up and heat is then transfered to the surface [18, 145] and can act in two ways: it can anneal ice at depth or release volatile compounds. What follows is an estimate of the temperature increase due to solid-state greenhouse effect using the model of Brown and Matson (1987) [18] and Spencer et al. (1989) [224]. Heat capacity and thermal conductivity are depth (and therefore temperature) dependent and are interpolated between pure water ice [213, 197] and an ammonia-water mixture [59, 136]. For Charon's visible albedo, a mixture of water ice and dark neutral absorber (dna) is used and the resulting flux-weighted visible albedo is $A \approx 0.38$, the bolometric albedo of Charon [44]. Assuming that the extinction coefficient of sunlight α is due to that of clear water ice, the mean absorption scale length $\overline{\zeta}$ is estimated as

$$\frac{1}{\overline{\zeta}} = \frac{\int_0^{+\infty} \alpha(\lambda)\{[1 - A(\lambda)]/[1 + A(\lambda)]\}\mathcal{F}_{\odot}(\lambda) d\lambda}{\int_0^{+\infty} \mathcal{F}_{\odot}(\lambda) d\lambda} \tag{5.4}$$

with a value of 12 m. If bubbles or impurities are present, the value will be lower (and so the temperature). Even considering an ice density of $\sim$0.5 g cm^{-3}, a very low thermal conductivity $\kappa \approx 100$ erg cm^{-1}s^{-1}K^{-1} typical of porous regolith and ignoring its scattering, the result is that temperature at depth increases by about 5 - 20 K, as long as the regolith extends to at least several meters. This means that, with this mechanism, ice on Charon cannot be warmer than 70 K and therefore cannot be annealed on a $< 10^5$ yr timescale or release water and ammonia.

Solid-state convection

Certain radionuclides in the interior of Charon can provide radiogenic heat that may drive solid-state convection of ice and bring nonirradiated crystalline ice to the surface. This requires that the Rayleigh number exceeds the critical value Ra$_c \sim 10^3$ [44] in the ice near the surface. The Rayleigh number is defined as

$$Ra = \frac{\alpha_T \Delta T g \rho (\Delta z)^3}{K\eta} = \frac{\alpha_T \rho^2 C_p}{\kappa^2 \eta} F g (\Delta z)^4, \tag{5.5}$$

where α_T is the thermal expansivity of the ice, η is its viscosity, g is the gravitational acceleration, $F = \kappa \frac{\Delta T}{\Delta z}$ is the heat flux driving the convection, ΔT is the temperature drop across the convecting ice, and Δz is the thickness of ice presumed to be convecting. For Charon, $g \approx 30$ cm s^{-2} and $F \approx 1$ erg cm^{-2}s^{-1} due to ^{40}K decay. The thermal conductivity of pure crystalline water ice is $\kappa = 567/T$ W m^{-1}K^{-1} [119], but can be decreased by factor of 2-3 if ammonia is added [136]. The heat capacity of I_h at temperatures 50-100 K lies in the range $C_p \approx (3.7-7.7)\times 10^6$ erg g^{-1}K^{-1} [213]. Thermal expansivities of I_h are typically $\alpha_T \sim 10^{-5}$ K^{-1} at $T \leq 273$ K, but decline steeply with decreasing temperature and becomes negative below about 60 K [198], making convection of water ice impossible where $T < 60$ K. Assuming $T \approx 100$ K, $\alpha = 10^{-5}$ K^{-1}, $C_p = 1 \times 10^7$ erg g^{-1}K^{-1}, $\kappa = 5.67$ W m^{-1}K^{-1}, and $\rho = 0.92$ g cm^{-3}, the condition for convection is that the viscosity is:

$$\eta \leq 8 \times 10^{16} \left(\frac{\Delta z}{100 \text{ km}} \right)^4 \text{poise},$$

using $\text{Ra}_c = 10^3$. The viscosity of pure I_h at 100 K is typically $\geq 10^{20}$ poise [45]. Impurities may lower the viscosity, in particular Durham et al. (1993) [50] found that adding ammonia with a mass fraction of 33% can reduce the viscosity to a value $\sim 10^{13}$ poise. Solid-state convection is therefore possible at depth where $T \geq 140$ K, but not on the surface and it must be concluded that this mechanism cannot bring crystalline water ice to Charon's surface.

Cryovolcanism

Since tidal heating is absent on Charon, if radiogenic heat from ^{40}K, ^{235}U, ^{238}U, and ^{232}Th is high enough, it can cause cryovolcanic phenomena. Assuming a olivine composition, the flux will be 4.4×10^{-8} erg s^{-1} per gram of rock [128]. Since Charon is composed of both rock and ice, and its average density is $\overline{\rho} = 1.71 \pm 0.08$ g cm^{-3} [214], the fraction of Charon's mass that is rock will be

$$f_{rock} = \frac{1 - \rho_{ice}/\overline{\rho}}{1 - \rho_{ice}/\rho_{rock}}. \tag{5.6}$$

Assuming again an olivine composition, with $\rho_{rock} = 3.3$ g cm^{-3}, the rock mass fraction results 0.64, with a rocky core of radius 420 km and an ice mantle thickness of 184 km. The total heat is $Q = 4.4 \times 10^{16}$ erg s^{-1} and the flux at the surface is $F(R_C) = Q/4\pi R_C^2 \approx 1.0$ erg cm^{-2}s^{-1}, while the flux at a radius r is $F(r) = F(R_C)R_C^2/r^2$. The temperature gradient is given by

$$\frac{\partial T}{\partial r} = -\frac{F(r)}{\kappa(T)}, \tag{5.7}$$

where $\kappa(T)$ is the temperature-dependent thermal conductivity of the ice, which, in this case, is $\kappa = \kappa_0 T_0/T$, where $\kappa_0 = 5.67$ W m^{-1}K^{-1} and $T_0 = 100$ K, leading to a temperature profile

$$T(r) = T_{surf}\exp\left[\frac{F(R_C)R_C}{\kappa_0 T_0}\left(\frac{R_C}{r} - 1\right)\right]. \tag{5.8}$$

Using $T_{surf} = 48$ K, the temperature at the base of the ice shell is then 77 K but, as the presence of ammonia hydrates on the surface suggests, the interior should be ammonia-rich that can lower the melting poing and the conductivity. As shown by Lorenz and Shandera (2001) [136], with solar abundances, ammonia lowers the thermal conductivity to ≈ 1.8 W m^{-1}K^{-1} and makes it constant on a wide range of temperatures, leading to the new temperature profile:

$$T(r) = T_{surf} + \frac{F(R_C)R_C}{\kappa_0}\left(\frac{R_C}{r} - 1\right) \tag{5.9}$$

from which, with an ammonia abundance of 15%, the temperature at the base of the ice shell is 198 K, too low to matain a liquid ocean, in the case of ice in steady-state.

However, since radiogenic heat decreases with time, this is not a situation in steady-state. Considering the higher heat flux present 4.5 Gyr ago [128], the results is that, for an ice that is 15% ammonia, 70% of the total ice would be melt. Therefore, ice on Charon was once melt and has been refreezing since then, but this process releases more heat and implies the need for a time-dependent calculation. In addition, the ammonia concentration has increased with time. If the ammonia mass fraction is $X \leq 0.32$, the first solids formed are pure water ice [92], while ammonia remains in liquid phase and, when $X > 0.33$, the first solid to form in the cooling liquid is now AMH, which is about 50% ammonia by weight, and therefore X now decreases. The consequence is that the freezing process drives the ammonia concentration to $X = 0.33$, which is the eutectic[1] value for a water-ammonia liquid, with a melting point of only 176 K. Therefore, if the initial abundance of ammonia was 15%, after the melting of half of the liquid, the abundance would be 0.33 and the deepest 10% would be still hot enough to be in liquid phase. In addition, another consequence of refreezing is that a fraction $(\rho_{liq}/\rho_{ice}) - 1 \sim 7\%$ must be displaced upward, also because ammonia lowers the density of

[1] A mixture of substances (in fixed proportions) that melts and solidifies at a single temperature that is lower than the melting points of the separate constituents or of any other mixture of them.

the liquid to about $\rho_{liq} = 1.00 - 0.38X$ g cm^{-3} [36]. The final fraction of liquid displaced is

$$f_d = \frac{\rho_{liq}}{\rho_{ice}} - 1 - \left(\frac{X - f_r}{\rho_{liq}}\right) \frac{\partial \rho_{liq}}{\partial X}, \tag{5.10}$$

where f_r is the fraction of ammonia removed from the ocean by either freezing or being removed to the surface by an eruption. Given a conduit, since this liquid always expands due to higher ammonia concentration, causing the density to lower, then pressure increases and drives the liquid to the surface [54]. Expansion originates cracks that, after reaching a critical length [35], propagate thanks to buoyancy effects and act as conduits. Since the ice shell contains rock and the liquid contains ammonia, the latter has a lower density and the crack can easily reach the surface in 1 hour [35]. The liquid may freeze by contact with the walls, reducing the ammonia concentration, but if $\sim$ 7% of the initial liquid reaches the surface on the same timescale as it freezes ($\sim$3 Gyr), the time-averaged rate at which ice is added to the surface is

$$\frac{dz}{dt} \sim \frac{0.7 f_d M_C (0.07)}{4\pi R_C^2 (3Gyr)} \sim 2 \text{ km Gyr}^{-1}, \tag{5.11}$$

which is about 20 cm over 10^5 yr for $X = 0$. If $0 < X \leq 0.33$, then 1 mm of crystalline water ice can be created on a timescale shorter than that needed by radiation to amorphize the ice. In particular, a value $f_d = 0.1\%$ is enough to account fo the crystalline water ice observed. The conclusion is that cryovolcanism is the process that must be continuously renewing Charon's surface.

5.5 Conclusion

Infrared spectra show several features about Charon: the surface is dominated by crystalline water ice and ammonia hydrates, the two hemispheres (sub-Pluto and anti-Pluto) appear to have different temperatures and ammonia hydration states and there is also a dark neutral absorber which has not been identified. Solar UV/visible radiation should quickly amorphize the ice, so there must be some mechanism that can crystallize ice on a shorter timescale. Calculations show that impacts (from both meteorites and micrometeorites), solid-state greenhouse and solid-state convection are unable to explain how 90% of the ice on Charon's surface is in the crystalline form. However, considering radiogenic heat and assuming that Charon formed with a significant fraction of ammonia, cryovolcanic processes could be a possible explanation. Calculations showed that the average depth probed by H and K wavelenghts can be covered in only 200 yr, during which only a fraction $< 0.5\%$ of the ice would be amorphized. This result is very important, because observations of Enceladus and Europa seemed to suggest that cryovolcanism could not be possible without tidal heating. This leads to the conclusion that cryovolcanic phenomena could be observed on other KBOs as well, where a great reservoir of liquid water could actually be found.

Chapter 6

Other satellites

The purpose of this chapter is to provide an overview of the other satellites of gaseous planets that have not been discussed before and where cryovolcanism is very likely to have happened. Information taken from G. Faure and T. M. Mensing, Introduction to Planetary Science [56].

6.1 Galileian satellites

6.1.1 Europa

Ice crust and ocean

Europa is the smallest and the brightest of the Galileian satellites (albedo of 64%), due to the icy and low-cratered surface. This implies that this satellite is active, probably because of tidal heating that keeps the crust partially liquid [181]. Underneath, there should be a liquid ocean between 80 and 170 km thick that acts as a reservoir from which water can be extruded and instantly solify at the surface. The surface is dominated by sets of intersecting double ridge systems, where the youngest ones cut over the others and, in general, is quite chaotic. Unlike other bodies of the Solar System, such as Io, there are no volcanoes or active plumes, and heat is probably loses heat by convection of water and by conduction through the ice. In this case, the more heat needs to be conducted to the surface, the thinner is the crust [67]. Some regions contain reddish brown deposits [149], probably consisting of salts that contain several metals (e.g., Na, Mg, K, Ca, Fe, etc.) and that are brought to the surface by the water rising through cracks in the crust, which probably sublimates at the surface. It has been proposed that living organisms could be found in Europa's global ocean and, in this case, organic materials should also be brought to the surface. The cracks, the double ridges and other features have formed due to tidal deformation and interaction with the underlying ocean, but several details about this interaction are still uncertain.

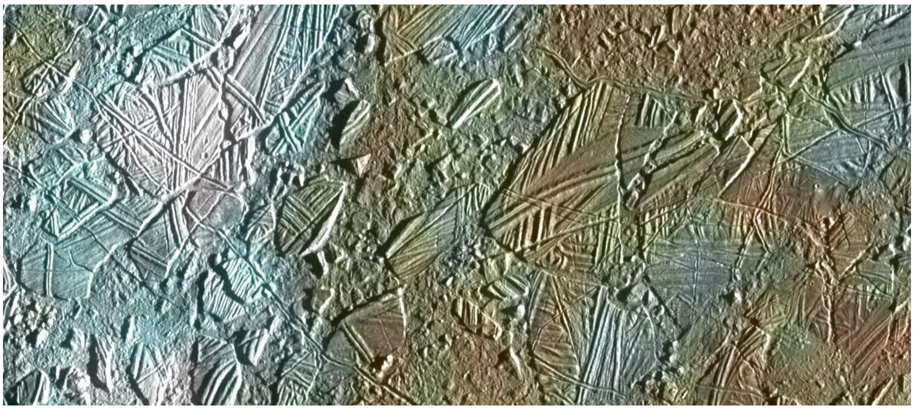

Figure 6.1: Chaotic terrain on Europa's surface. As explained in Section 6.1.1, the crater density is very low, demonstrating that there has been a relatively recent surface renewal.

Impact craters

The age of the surface estimated by crater density is 50 Myr [259], and the shape of these craters suggests that a weak layer, such as a global ocean, must be present at depth. Cryovolcanic activity and breakthrough of water have destroyed the majority of these craters. What's more, the sublimation of exposed ice further contributes to the disappearing of the craters. The lack of craters, which have been caused by impacts of comets, asteroids and other fragments, is a feature that is not common among icy satellites.

6.1.2 Ganymede

The surface of Ganymede is divided in dark regions older than 4 Gyr (34% of the total surface) and light regions (66%), which could be between 3.1 and 3.7 Gyr old or only 1 Gyr old. The crust of Ganymede must be thicker than that of Europa, because the impactors did not break through it and because the terrain is not chaotic and does not show reddish brown salt deposits. What's more, tidal heating is surely weaker on Ganymede and this satellite does now show signs of activity, volcanoes, plumes, or geysers. The thickness of the crust has been estimated to be 170 km, with an underlying ocean like on Europa.

Rejuvenation

Even though there are no signs of current activity, the lighter regions must have been rejuvenated at some point in Ganymede's history, since they show sets of parallel ridges and valleys. These features do not seem to be tidal fractures, but just normal faults or tilted blocks of the ice crust. Some bands of grooved terrain cut cross other bands, showing an evolution in time. This is probably due to an episode of violent deformation, presumably because, in Gaymede's early history, ice at depth was warmer and therefore more deformable, in contrast with the brittle surface ice. This could have caused some sort of cryovolcanic activity in the distant past, although this kind of activity is no longer taking place today [179].

6.1.3 Callisto

Callisto is not heated by tides and this is confirmed by its low albedo (17%), which proves that the surface has never been rejuvenated. Moreover, Callisto was not hot enough to differentiated and therefore did not form an ice crust like Europa and Ganymede. The surface appears to have experienced sublimation of the ice, which left impurities and that was more efficient on Callisto than on Europa, since Callisto has a lower albedo and therefore has a higher surface temperature [84]. The impurities and the thickness of the covering sediment slow down the rate of sublimation, forming ridges and eroding small impact craters. Since the surface has not been rejuvenated by cryovolcanic activity, sublimation of the ice is the dominant process that shapes Callisto's surface.

6.2 Saturnian satellites

6.2.1 Tethys and Dione

Both Tethys and Dione have both lightly and heavily cratered regions, showing evidence of geological activity. Tethys posses a 40 km wide crater called Odysseus (visible in figure 6.2), which has been caused by a dramatic impact. The plain found at the antipode of this crater is very lightly cratered and therefore must have been rejuvenated by the extrusion of water lava. What's more, centered on the Odysseus crater, is a heavily cratered region with a system of rift valleys called Ithaca chasma. The impact that formed the Odysseus basin is thought to have caused both the formation of the rift valleys and the cryovolcanic activity on the antipodal point.

Dione also shows a lightly cratered region that stretches from pole to pole and a system of valleys that goes from the poles to the mid-latitudes. Both these regions suggest cryovolcanic activity, in particular the valleys are thought to be the result of tectonic activity or channels were cryolava once flowed. However, both satellites seem to have experienced activity in their early history and appear totally inactive today.

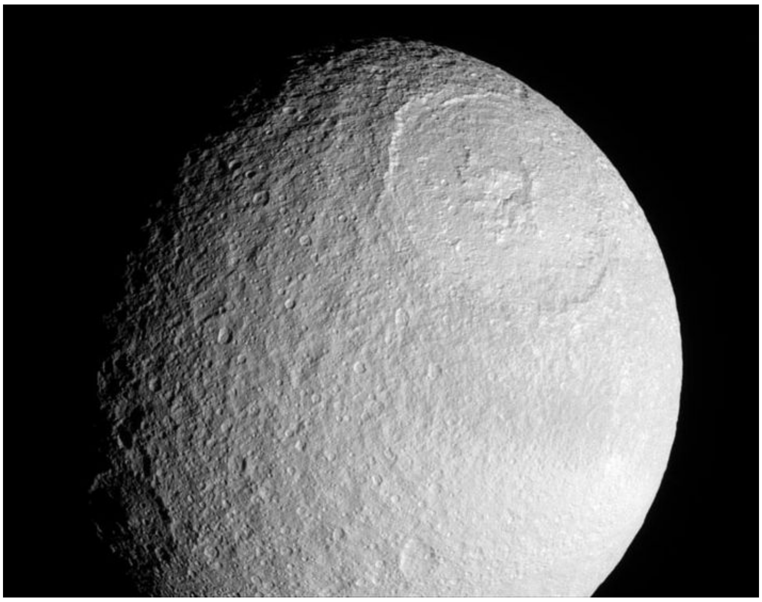

Figure 6.2: The Odysseus basin on Tethys.

6.2.2 Rhea and Hyperion

Although Rhea is much bigger than Tethys and Dione, and should thus have remained hot for a longer time, it has been observed that its surface is heavily cratered, implying that no activity has taken place. The low density implies a low abundance of rocks (probably 20% by volume) that does not provide enough radiogenic heat, and tidal heating is also negligible due to the low eccentricity, the great distance from Saturn, and the lack of any resonance. However, the surface of Rhea shows topographic features, such as ridges, that may be due to a phase transformation that led the ice in the interior to become a dense polymorph called ice II. This causes compression that modifies the surface, and generates those ridges, and also prevents the formation of vents from which cryomagma could have been extruded [152]. The craters are mostly small and are thought to be due to ejecta from Hyperion, which was presumably struck by several objects, that caused it to have the irregular shape seen today. Most of these ejecta could have been captured by the massive Titan, while the others might have end up striking Rhea's surface or being incorporated into the rings of Saturn [152].

Hyperion has a much lower albedo than Rhea (30% against 60%) and is heavily cratered, suggesting that, in spite of its high eccentricity, it did not experience surface renewal.

6.3 Uranian satellites

6.3.1 Miranda

Miranda contains three rectangular coronas which are lightly cratered and are surrounded by a heavily cratered terrain, therefore the coronas are very young. This satellite is the closest to Uranus, which captured many objects that destroyed Miranda so that it reassembed as seen today [180]. These impacts could have provided enough heat to cause differentiation and cryovolcanism, which appears to be absent today.

6.3.2 Ariel

Ariel has a very dark surface given by organic matter and amorphouse carbon, as well as young and bright craters. In the northern hemisphere there are features which prove that this satellite was tectonically active and that water-ammonia and water-methane lava did flow. Presumably, the needed heat came from tidal friction caused by a more eccentric orbit in the past.

6.3.3 Umbriel

Umbriel has a very low albedo and a heavily cratered surface that has not been rejuvenated by cryovolcanic activity. The dark color is due to organic matter and amorphous carbon, just like Ariel. Even if it is not certain, Umbriel could have been geologically active in the past, but so far it is not know whether it was able to differentiate.

6.3.4 Titania

Titania has a heavily cratered surface with steep-sided rift valleys as on Ariel. However, Titania is brighter than Umbriel because its organic-rich layer is not as thick (or not as dark) as the one on Umbriel. This seems to point out that Titania was once tectonically active and that parts of its surface were rejuvenated by the eruption of lava flows composed of water and methane.

6.3.5 Oberon

Oberon is very similar to Titania and, just like Titania, shows signs of tectonical activity that formed rift valleys and therefore allowed lava flows of water-ammonia to be erupted. The heat needed for this presumably came from tidal friction, as seen for the other classical satellites of Uranus.

6.4 Neptunian satellites

The smaller satellites are surely inactive, despite being composed of volatile compounds, due to the low S/V ratio and the absence of tidal heating, the latter is a consequence of the low eccentricities and the spin-orbit coupling.

6.4.1 Triton

Triton is the biggest Neptunian satellite and is composed of ices of volatile compounds [38] that cause a very high albedo of 75%. Voyager 2 showed that the surface is lightly cratered and has therefore been renewed. The southern hemisphere contains particular features: a terrain called "cantaloupe terrain" that has never been observed on other icy satellites and that includes intersecting sets of double ridges, valleys, and irregular hills and planes. There are also deposits irregularly distributed that are light-colored, have formed due to condensation of volatile compounds and have covered the impact craters. Close to the deposits, some plumes have been observed which reach heights of 8 km and are mainly composed of nitrogen gas that later solifies as snow, due to expansion and cooling. Given the phase diagram of N, two possible paths are possible, in order to explain this phenomenum: one considers a decrease in pressure on solid nitrogen in the subsurface, the other implies an increase in temperature at nearly constant pressure. Some plains like the Ruach planitia seem to be formed by the extrusion of cryomagma, freezing, remelting and collapse. Since they often contain a central impact crater, the impact itself may play a role in this process. The heat needed for these processes could be due to Triton's origin: it is thought to be a KBO captured by Neptune in ancient times, so it could have initially had a very eccentric orbit. Then, tidal friction may have caused it to become circular, generating a high heat flux. In this scenario, the surface can have been rejuvenated by either cryvolcanism or global meltdown. The emission of liquid nitrogen observed today indicates that there is still heat that drives geological activity.

Chapter 7

Conclusions

As shown in this work, the study of volcanic and cryovolcanic phenomena is a very important matter. In particular, this kind of phenomena is strongly linked to other fields of planetary science. Volcanic and cryovolcanic phenomena are, in general, what links surface features to internal processes and, provide an important way to determine the evolution of the planets and satellites on which they are observed. For example, as pointed out in Chapter 2, the observation of volcanic processes can help us improve rheological models, which can, for example, be used to describe Earth's interior thus leading to a better understanding of our own planet. This is also linked, as shown in Section 2.6.4, to the possible orbital evolution of satellites and thus to the formation of protosolar and protoplanetary disks. Furthermore, these models can also be applied to exoplanets, in order to study volcanically active worlds in other solar systems. As shown in Section 3.3, cryovolcanic and volcanic phenomena are definitely linked to the evolution of the atmosphere, since the lack of these processes on Titan would have determined the absence of methane in its atmosphere. Section 4.2.6 describes the most remarkable example of how cryovolcanic process on a small satellite can affect other satellites and even the impressive Saturnian ring system. Enceladus is the most important cryovolcanically active known bod, and the study of this satellite can improve the understanding of several chemical processes and of how tidal heating affects cold and small satellites. Chapter 5 showed two important aspects: first, cryovolcanism is possible even on the far, small, and extremely cold KBOs; second, these processes can take place even in the absence of tidal heating, provided that another important heat source is present (e.g., radiogenic heat). This suggests that liquid water can actually be found even at those great distances from the Sun, where the presence of liquid water was before unthinkable. In the end, Chapter 6 showed that, in general, volcanic and cryovolcanic processes are so common in the Solar System, or were so in the past, that it is impossible to deeply understand the history of our Solar System without a profound knowledge of this kind of phenomena.

There is a growing interest towards the bond between volcanic and cryovolcanic phenomena and exobiology: since the presece of these phenomena implies the presence of heat and, in the case of cryovolcanism, of liquid water, somewhere these processes may create favourable conditions for the presence of life. For example, the hypothesis of the presence of simple life forms on Europa dates back to 1979. Moreover, the sustainability of life on volcanically and cryovolcanically active worlds is of particular interest in the scenario of a possible future colonization of the Solar System.

Improvements in this field can be achieved in several ways. As already mentioned, laboratory studies on a wide range of materials and the improvement of rheological models are key factors. Moreover, in order to understand cryovolcanic processes, it is important to better study thermodynamic and chemical processes involving water, ammonia, salts and hydrocarbons. As shown in Chapter 3, topographic data from photogrammetry can be very useful to understand the structure of certain surface features, and this can help determine the effects of volcanic and cryovolcanic phenomena on the surface of planets and satellites. In general, more observations are definitely needed. For example, the Uranian and Neptunian systems have not been observed with the same care that has been used in observing the Jovian and Saturnian systems, and this will require more attention in the planning of future exploration missions. In addition, as showed in Chapter 5, further observations of KBOs could also reveal many surprises. Future observations of Mercury with the BepiColombo mission could reveal interesting details about the possible Mercurian volcanic activity in the very distant past, right after the formation of this planet. Also, more data and observations about Venus are definitely needed: these are made very difficult by the thick atmosphere and by the tough surface conditions, but this planet surely experienced volcanic activity in the geologically recent past that left traces which need to be investigated. Mars also seems to have experienced volcanic activity and, in this particular case, it is important to determine whether this activity could still be present, especially because this planet seems to be the most suitable for human colonization.

Ringraziamenti

Vorrei innanzitutto ringraziare il professor Casotto per aver accettato di essere il mio relatore e per aver dedicato a questo progetto parte del suo tempo, aiutandomi in ogni modo che gli fosse possibile. Ringrazio tutti i professori del Dipartimento di Astronomia con cui ho avuto a che fare, per aver contribuito alla mia crescita come studente. Ringrazio Francesca, la mia ragazza, per essermi stata vicino e avermi sostenuto in questi anni di università, poiché senza di lei sarebbe stato tutto notevolmente più difficile. Ringrazio tutta la mia famiglia, i miei genitori, i miei fratelli, i miei nonni e i miei zii per aver sempre e indiscutibilmente creduto in me. Ringrazio tutti i miei amici, i miei compagni di liceo, i miei ex compagni di squadra e i miei compagni di università per i bei momenti passati insieme.

Bibliography

[1] O. Abramov and J. R. Spencer. Endogenic heat from Enceladus' south polar fractures: New observations, and models of conductive surface heating. *Icarus*, 199:189–196, January 2009.

[2] M. H. Acuna, J. E. P. Connerney, N. F. Ness, R. P. Lin, D. Mitchell, C. W. Carlson, J. McFadden, K. A. Anderson, H. Reme, C. Mazelle, D. Vignes, P. Wasilewski, and P. Cloutier. Global Distribution of Crustal Magnetization Discovered by the Mars Global Surveyor MAG/ER Experiment. *Science*, 284:790, April 1999.

[3] M. F. Ashby and R. A. Verrall. Micromechanisms of flow and fracture, and their relevance to the rheology of the upper mantle. *Philosophical Transactions of the Royal Society of London A: Mathematical, Physical and Engineering Sciences*, 288(1350):59–95, 1978.

[4] J. W. Barnes, J. Bow, J. Schwartz, R. H. Brown, J. M. Soderblom, A. G. Hayes, G. Vixie, S. Le Mouélic, S. Rodriguez, C. Sotin, R. Jaumann, K. Stephan, L. A. Soderblom, R. N. Clark, B. J. Buratti, K. H. Baines, and P. D. Nicholson. Organic sedimentary deposits in Titan's dry lakebeds: Probable evaporite. *Icarus*, 216:136–140, November 2011.

[5] A. C. Barr. Mobile lid convection beneath Enceladus' south polar terrain. *Journal of Geophysical Research (Planets)*, 113:E07009, July 2008.

[6] A. C. Barr and W. B. McKinnon. Convection in Enceladus' ice shell: Conditions for initiation. *Geophysical Research Letters*, 34:L09202, May 2007.

[7] A. C. Barr and L. J. Preuss. On the origin of south polar folds on Enceladus. *Icarus*, 208:499–503, July 2010.

[8] J. M. Bauer, T. L. Roush, T. R. Geballe, K. J. Meech, T. C. Owen, W. D. Vacca, J. T. Rayner, and K. T. C. Jim. The Near Infrared Spectrum of Miranda: Evidence of Crystalline Water Ice. *Icarus*, 158:178–190, July 2002.

[9] C. Béghin, C. Sotin, and M. Hamelin. Titan's native ocean revealed beneath some 45km of ice by a Schumann-like resonance. *Comptes Rendus Geoscience*, 342:425–433, June 2010.

[10] J. E. Bertie and M. M. Morrison. The infrared spectra of the hydrates of ammonia, $NH_3 \cdot H_2O$ and $NH_3 \cdot 2H_2O$ at 95 degK. *Journal of Chemical Physics*, 73:4832–4837, November 1980.

[11] J. E. Bertie and M. R. Shehata. Ammonia dihydrate: Preparation, x-ray powder diffraction pattern and infrared spectrum of $NH_3 \cdot 2H_2O$ at 100 K. *The Journal of Chemical Physics*, 81:27–30, July 1984.

[12] C. J. Bierson and F. Nimmo. A test for io's magma ocean: Modeling tidal dissipation with a partially molten mantle. *Journal of Geophysical Research: Planets*, 121(11):2211–2224, 2016. 2016JE005005.

[13] M. T. Bland, R. A. Beyer, and A. P. Showman. Unstable extension of Enceladus' lithosphere. *Icarus*, 192:92–105, December 2007.

[14] M. T. Bland, K. N. Singer, W. B. McKinnon, and P. M. Schenk. Enceladus' extreme heat flux as revealed by its relaxed craters. *Geophysical Research Letters*, 39:L17204, September 2012.

[15] M. E. Brown and W. M. Calvin. Evidence for Crystalline Water and Ammonia Ices on Pluto's Satellite Charon. *Science*, 287:107–109, January 2000.

[16] R. H. Brown, R. N. Clark, B. J. Buratti, D. P. Cruikshank, J. W. Barnes, R. M. E. Mastrapa, J. Bauer, S. Newman, T. Momary, K. H. Baines, G. Bellucci, F. Capaccioni, P. Cerroni, M. Combes, A. Coradini, P. Drossart, V. Formisano, R. Jaumann, Y. Langevin, D. L. Matson, T. B. McCord, R. M. Nelson, P. D. Nicholson, B. Sicardy, and C. Sotin. Composition and Physical Properties of Enceladus' Surface. *Science*, 311:1425–1428, March 2006.

[17] R. H. Brown, D. P. Cruikshank, A. T. Tokunaga, R. G. Smith, and R. N. Clark. Search for volatiles on icy satellites. I - Europa. *Icarus*, 74:262–271, May 1988.

[18] R. H. Brown and D. L. Matson. Thermal effects of insolation propagation into the regoliths of airless bodies. *Icarus*, 72:84–94, October 1987.

[19] M. W. Buie and W. M. Grundy. The Distribution and Physical State of H_2O on Charon. *Icarus*, 148:324–339, December 2000.

[20] M. W. Buie, D. J. Tholen, and K. Horne. Albedo maps of Pluto and Charon - Initial mutual event results. *Icarus*, 97:211–227, June 1992.

[21] M. Běhounková, G. Tobie, G. Choblet, and O. Čadek. Coupling mantle convection and tidal dissipation: Applications to Enceladus and Earth-like planets. *Journal of Geophysical Research (Planets)*, 115:E09011, September 2010.

[22] M. Běhounková, G. Tobie, G. Choblet, and O. Čadek. Tidally-induced melting events as the origin of south-pole activity on Enceladus. *Icarus*, 219:655–664, June 2012.

[23] R. M. Canup and W. R. Ward. Formation of the Galilean satellites: Conditions of accretion. *The Astronomical Journal*, 124(6):3404, 2002.

[24] R. M. Canup and W. R. Ward. A common mass scaling for satellite systems of gaseous planets. *Nature*, 441:834–839, June 2006.

[25] R. M. Canup and W. R. Ward. *Origin of Europa and the Galilean Satellites*, page 59. 2009.

[26] T. A. Cassidy and R. E. Johnson. Collisional spreading of Enceladus' neutral cloud. *Icarus*, 209:696–703, October 2010.

[27] J. C. Castillo-Rogez, M. Efroimsky, and V. Lainey. The tidal history of Iapetus: Spin dynamics in the light of a refined dissipation model. *Journal of Geophysical Research: Planets*, 116(E9):n/a–n/a, 2011. E09008.

[28] S. Charnoz, A. Crida, J. C. Castillo-Rogez, V. Lainey, L. Dones, Ö. Karatekin, G. Tobie, S. Mathis, C. Le Poncin-Lafitte, and J. Salmon. Accretion of Saturn's mid-sized moons during the viscous spreading of young massive rings: Solving the paradox of silicate-poor rings versus silicate-rich moons. *Icarus*, 216:535–550, December 2011.

[29] E. M. A. Chen and F. Nimmo. Obliquity tides do not significantly heat Enceladus. *Icarus*, 214:779–781, August 2011.

[30] M. Choukroun, O. Grasset, G. Tobie, and C. Sotin. Stability of methane clathrate hydrates under pressure: Influence on outgassing processes of methane on Titan. *Icarus*, 205:581–593, February 2010.

[31] G. C. Collins and J. C. Goodman. Enceladus' south polar sea. *Icarus*, 189:72–82, July 2007.

[32] K. Consani and G. C. Pimentel. Infrared spectra of the clathrate hydrates of acetylene and of acetylene/acetone. *The Journal of Physical Chemistry*, 91(2):289–293, 1987.

[33] J. C. Cook, S. J. Desch, T. L. Roush, C. A. Trujillo, and T. R. Geballe. Near-Infrared Spectroscopy of Charon: Possible Evidence for Cryovolcanism on Kuiper Belt Objects. *The Astrophysical Journal*, 663:1406–1419, July 2007.

[34] J. F. Cooper, E. R. Christian, J. D. Richardson, and C. Wang. Proton Irradiation of Centaur, Kuiper Belt, and Oort Cloud Objects at Plasma to Cosmic Ray Energy. *Earth Moon and Planets*, 92:261–277, June 2003.

[35] G. D. Crawford and D. J. Stevenson. Gas-driven water volcanism in the resurfacing of Europa. *Icarus*, 73:66–79, jan 1988.

[36] S. K. Croft, J. I. Lunine, and J. Kargel. Equation of state of ammonia-water liquid - Derivation and planetological applications. *Icarus*, 73:279–293, February 1988.

[37] E. Crow-Willard and R. T. Pappalardo. Global Geological Mapping of Enceladus. In *EPSC-DPS Joint Meeting 2011*, page 635, October 2011.

[38] D. P. Cruikshank, R. H. Brown, L. P. Giver, and A. T. Tokunaga. Triton - Do we see to the surface? *Science*, 245:283–286, July 1989.

[39] D. P. Cruikshank, T. C. Owen, C. Dalle Ore, T. R. Geballe, T. L. Roush, C. de Bergh, S. A. Sandford, F. Poulet, G. K. Benedix, and J. P. Emery. A spectroscopic study of the surfaces of Saturn's large satellites: H_2O ice, tholins, and minor constituents. *Icarus*, 175:268–283, May 2005.

[40] E. N. da C. Andrade. On the viscous flow in metals, and allied phenomena. *Proceedings of the Royal Society of London A: Mathematical, Physical and Engineering Sciences*, 84(567):1–12, 1910.

[41] E. Dartois, L. d'Hendecourt, W. Thi, K. M. Pontoppidan, and E. F. van Dishoeck. Combined VLT ISAAC/ISO SWS spectroscopy of two protostellar sources. The importance of minor solid state features. *Astronomy and Astrophysics*, 394:1057–1068, November 2002.

[42] G. H. Darwin. I. on the bodily tides of viscous and semi-elastic spheroids, and on the ocean tides upon a yielding nucleus. *Philosophical Transactions of the Royal Society of London*, 170:1–35, 1879.

[43] A. G. Davies, L. Keszthelyi, and A. S. McEwen. Estimating eruption temperature from thermal emission spectra of lava fountain activity in the Erta'Ale (Ethiopia) volcano lava lake: Implications for observing Io's volcanoes. *Geophysical Research Letters*, 38(21):n/a–n/a, 2011. L21308.

[44] I. de Pater and J. J. Lissauer. *Planetary Sciences*. December 2001.

[45] F. Deschamps and C. Sotin. Thermal convection in the outer shell of large icy satellites. *Journal of Geophysical Research*, 106:5107–5121, March 2001.

[46] M. K. Dougherty, L. W. Esposito, and S. M. Krimigis. *Saturn from Cassini-Huygens*. Springer Verlag, 2009.

[47] L. G. Dowell and A. P. Rinfret. Low-Temperature Forms of Ice as Studied by X-Ray Diffraction. *Nature*, 188:1144–1148, December 1960.

[48] C. Dumas, R. J. Terrile, R. H. Brown, G. Schneider, and B. A. Smith. Hubble Space Telescope NICMOS Spectroscopy of Charon's Leading and Trailing Hemispheres. *The Astronomical Journal*, 121:1163–1170, February 2001.

[49] D. D. Durda and S. A. Stern. Collision Rates in the Present-Day Kuiper Belt and Centaur Regions: Applications to Surface Activation and Modification on Comets, Kuiper Belt Objects, Centaurs, and Pluto-Charon. *Icarus*, 145:220–229, May 2000.

[50] W. B. Durham, S. H. Kirby, and L. A. Stern. Flow of ices in the ammonia-water system. *Journal of Geophysical Research*, 98:17667–17682, October 1993.

[51] M. Efroimsky. Tidal dissipation compared to seismic dissipation: In small bodies, earths, and super-earths. *The Astrophysical Journal*, 746(2):150, 2012b.

[52] J. P. Emery, D. M. Burr, D. P. Cruikshank, R. H. Brown, and J. B. Dalton. Near-infrared (0.8-4.0 μm) spectroscopy of Mimas, Enceladus, Tethys, and Rhea. *Astronomy and Astrophysics*, 435:353–362, May 2005.

[53] L. W. Esposito, J. E. Colwell, K. Larsen, W. E. McClintock, A. I. F. Stewart, J. T. Hallett, D. E. Shemansky, J. M. Ajello, C. J. Hansen, A. R. Hendrix, R. A. West, H. U. Keller, A. Korth, W. R. Pryor, R. Reulke, and Y. L. Yung. Ultraviolet Imaging Spectroscopy Shows an Active Saturnian System. *Science*, 307:1251–1255, February 2005.

[54] S. A. Fagents. Considerations for effusive cryovolcanism on Europa: The post-Galileo perspective. *Journal of Geophysical Research (Planets)*, 108:5139, December 2003.

[55] S. A. Fagents, R. Greeley, R. J. Sullivan, R. T. Pappalardo, L. M. Prockter, and The Galileo SSI Team. Cryomagmatic Mechanisms for the Formation of Rhadamanthys Linea, Triple Band Margins, and Other Low-Albedo Features on Europa. *Icarus*, 144:54–88, March 2000.

[56] G. Faure and T. M. Mensing. *Introduction to Planetary Science: The Geological Perspective*. Springer Verlag, 2007.

[57] W. M. Folkner, C. F. Yoder, D. N. Yuan, E. M. Standish, and R. A. Preston. Interior Structure and Seasonal Mass Redistribution of Mars from Radio Tracking of Mars Pathfinder. *Science*, 278:1749, December 1997.

[58] A. Fortes. *Computational and experimental studies of solids in the ammonia-water system*. PhD thesis, University of London, University College London (United Kingdom, 2004.

[59] A. D. Fortes, I. G. Wood, J. P. Brodholt, and L. Vočadlo. The structure, ordering and equation of state of ammonia dihydrate ($NH_3{\cdot}2H_2O$). *Icarus*, 162:59–73, March 2003.

[60] A.D. Fortes, P.M. Grindrod, S.K. Trickett, and L. Voadlo. Ammonium sulfate on Titan: Possible origin and role in cryovolcanism. *Icarus*, 188(1):139 – 153, 2007.

[61] R. Freedman and W. J. Kaufmann. *Universe, 6th edition*. 2002.

[62] B. Giese, H. Hussmann, T. Roatsch, P. Helfenstein, P. C. Thomas, and G. Neukum. Enceladus: Evidence for librations forced by Dione. In *EPSC-DPS Joint Meeting 2011*, page 976, October 2011.

[63] B. Giese, R. Wagner, H. Hussmann, G. Neukum, J. Perry, P. Helfenstein, and P. C. Thomas. Enceladus: An estimate of heat flux and lithospheric thickness from flexurally supported topography. *Geophysical Research Letters*, 35:L24204, December 2008.

[64] Gustavo Gioia, Pinaki Chakraborty, Stephen Marshak, and Susan W. Kieffer. Unified model of tectonics and heat transport in a frigid Enceladus. *Proceedings of the National Academy of Sciences*, 104(34):13578–13581, 2007.

[65] D. L. Goldsby and D. L. Kohlstedt. Superplastic deformation of ice: Experimental observations. *Journal of Geophysical Research: Solid Earth*, 106:11, June 2001.

[66] C. Gosmeyer, M. M. Hedman, J. A. Burns, and P. D. Nicholson. Variability in the Particle Plume of Saturn's Moon Enceladus. In *American Astronomical Society Meeting Abstracts #221*, volume 221 of *American Astronomical Society Meeting Abstracts*, page 353.16, January 2013.

[67] R. Greenberg. *Europa - the Ocean Moon : search for an alien biosphere.* 2005.

[68] T. T. Gribb and R. F. Cooper. Low-frequency shear attenuation in polycrystalline olivine: Grain boundary diffusion and the physical significance of the andrade model for viscoelastic rheology. *Journal of Geophysical Research: Solid Earth*, 103(B11):27267–27279, 1998.

[69] E. Groten, S. M. Molodenski, and V. N. Zharkov. On the Theory of Mars' Forced Nutation. *Astronomical Journal*, 111:1388, March 1996.

[70] W. M. Grundy, M. W. Buie, J. A. Stansberry, J. R. Spencer, and B. Schmitt. Near-Infrared Spectra of Icy Outer Solar System Surfaces: Remote Determination of H $_2$O Ice Temperatures. *Icarus*, 142:536–549, December 1999.

[71] W. M. Grundy and B. Schmitt. The temperature-dependent near-infrared absorption spectrum of hexagonal H_2O ice. *Journal of Geophysical Research*, 103:25809–25822, November 1998.

[72] W. M. Grundy, B. Schmitt, and E. Quirico. The Temperature-Dependent Spectrum of Methane Ice I between 0.7 and 5 μm and Opportunities for Near-Infrared Remote Thermometry. *Icarus*, 155:486–496, February 2002.

[73] C. A. Gueymard. Reference solar spectra: Their evolution, standardization issues, and comparison to recent measurements. *Advances in Space Research*, 37:323–340, 2006.

[74] A. A. S. Gulbis, J. L. Elliot, M. J. Person, E. R. Adams, B. A. Babcock, M. Emilio, J. W. Gangestad, S. D. Kern, E. A. Kramer, D. J. Osip, J. M. Pasachoff, S. P. Souza, and T. Tuvikene. Charon's radius and atmospheric constraints from observations of a stellar occultation. *Nature*, 439:48–51, January 2006.

[75] R. M. Haberle, M. M. Joshi, J. R. Murphy, J. R. Barnes, J. T. Schofield, G. Wilson, M. Lopez-Valverde, J. L. Hollingsworth, A. F. C. Bridger, and J. Schaeffer. General circulation model simulations of the Mars Pathfinder atmospheric structure investigation/meteorology data. *Journal of Geophysical Research*, 104:8957–8974, April 1999.

[76] L. Han, G. Tobie, and A. P. Showman. The impact of a weak south pole on thermal convection in Enceladus' ice shell. *Icarus*, 218:320–330, March 2012.

[77] C. J. Hansen, D. E. Shemansky, L. W. Esposito, A. I. F. Stewart, B. R. Lewis, J. E. Colwell, A. R. Hendrix, R. A. West, J. H. Waite, Jr., B. Teolis, and B. A. Magee. The composition and structure of the Enceladus plume. *Geophysical Research Letters*, 38:L11202, June 2011.

[78] G. B. Hansen. Spectral absorption of solid CO_2 from the ultraviolet to the far-infrared. *Advances in Space Research*, 20:1613–1616, January 1997a.

[79] G. B. Hansen. The infrared absorption spectrum of carbon dioxide ice from 1.8 to 333 μm. *Journal of Geophysical Research*, 102:21569–21588, September 1997b.

[80] V. L. Hansen, B. K. Banks, and R. R. Ghent. Tessera terrain and crustal plateaus, Venus. *Geology*, 27:1071, December 1999.

[81] B. Hapke. Bidirectional reflectance spectroscopy. I - Theory. *Journal of Geophysical Research*, 86:3039–3054, April 1981.

[82] W. K. Hartmann. Martian cratering VI: Crater count isochrons and evidence for recent volcanism from Mars Global Surveyor. *Meteoritics & Planetary Science*, 34(2):167–177, 1999.

[83] W. K Hartmann. *A traveler's guide to Mars: the mysterious landscapes of the Red Planet*. Workman Publishing, 2003.

[84] W. K. Hartmann. *Moons and planets*. 2005.

[85] P. Hartogh, E. Lellouch, R. Moreno, D. Bockelée-Morvan, N. Biver, T. Cassidy, M. Rengel, C. Jarchow, T. Cavalié, J. Crovisier, F. P. Helmich, and M. Kidger. Direct detection of the Enceladus water torus with Herschel. *Astronomy and Astrophysics*, 532:L2, August 2011.

[86] J. W. Head and R. T. Pappalardo. Brine mobilization during lithospheric heating on Europa: Implications for formation of chaos terrain, lenticula texture, and color variations. *Journal of Geophysical Research*, 104:27143–27156, 1999.

[87] J. W. Head and L. Wilson. Magma reservoirs and neutral buoyancy zones on Venus - Implications for the formation and evolution of volcanic landforms. *Journal of Geophysical Research*, 97:3877–3903, March 1992.

[88] M. M. Hedman, P. D. Nicholson, M. R. Showalter, R. H. Brown, B. J. Buratti, and R. N. Clark. Spectral Observations of the Enceladus Plume with Cassini-Vims. *The Astrophysical Journal*, 693:1749–1762, March 2009.

[89] H.-G. Heide. Observations on ice layers. *Ultramicroscopy*, 14(3):271 – 278, 1984.

[90] W. G. Henning and T. Hurford. Tidal heating in multilayered terrestrial exoplanets. *The Astrophysical Journal*, 789(1):30, 2014.

[91] W. G. Henning, R. J. O'Connell, and D. D. Sasselov. Tidally heated terrestrial exoplanets: Viscoelastic response models. *The Astrophysical Journal*, 707(2):1000, 2009.

[92] D. L. Hogenboom, J. S. Kargel, G. J. Consolmagno, T. C. Holden, L. Lee, and M. Buyyounouski. The Ammonia-Water System and the Chemical Differentiation of Icy Satellites. *Icarus*, 128:171–180, July 1997.

[93] C. J. A. Howett, J. R. Spencer, J. Pearl, and M. Segura. Thermal inertia and bolometric Bond albedo values for Mimas, Enceladus, Tethys, Dione, Rhea and Iapetus as derived from Cassini/CIRS measurements. *Icarus*, 206:573–593, April 2010.

[94] C. J. A. Howett, J. R. Spencer, J. Pearl, and M. Segura. High heat flow from Enceladus' south polar region measured using 10-600 cm^{-1} Cassini/CIRS data. *Journal of Geophysical Research (Planets)*, 116:E03003, March 2011.

[95] D. H. Humes. Results of pioneer 10 and 11 meteoroid experiments: Interplanetary and near-saturn. *Journal of Geophysical Research: Space Physics*, 85(A11):5841–5852, 1980.

[96] T. A. Hurford, P. Helfenstein, G. V. Hoppa, R. Greenberg, and B. G. Bills. Eruptions arising from tidally controlled periodic openings of rifts on Enceladus. *Nature*, 447:292–294, May 2007.

[97] H. Hussmann and T. Spohn. Thermal-orbital evolution of Io and Europa. *Icarus*, 171(2):391 – 410, 2004.

[98] L. Iess, R. A. Jacobson, M. Ducci, D. J. Stevenson, J. I. Lunine, J. W. Armstrong, S. W. Asmar, P. Racioppa, N. J. Rappaport, and P. Tortora. The Tides of Titan. *Science*, 337:457, July 2012.

[99] L. Iess, N. J. Rappaport, R. A. Jacobson, P. Racioppa, D. J. Stevenson, P. Tortora, J. W. Armstrong, and S. W. Asmar. Gravity field, shape, and moment of inertia of titan. *Science*, 327(5971):1367–1369, 2010.

[100] A. P. Ingersoll and S. P. Ewald. Total particulate mass in Enceladus plumes and mass of Saturn's E ring inferred from Cassini ISS images. *Icarus*, 216:492–506, December 2011.

[101] A. P. Ingersoll and A. A. Pankine. Subsurface heat transfer on Enceladus: Conditions under which melting occurs. *Iicarus*, 206:594–607, April 2010.

[102] B. Jackson, R. Greenberg, and R. Barnes. Tidal heating of extrasolar planets. *The Astrophysical Journal*, 681(2):1631, 2008.

[103] I. Jackson. Progress in the experimental study of seismic wave attenuation. *Annual Review of Earth and Planetary Sciences*, 21(1):375–406, 1993.

[104] I. Jackson, U. H. Fau, J. D. Fitz Gerald, and B. H. Tan. Shear wave attenuation and dispersion in melt-bearing olivine polycrystals: 1. specimen fabrication and mechanical testing. *Journal of Geophysical Research: Solid Earth*, 109(B6):n/a–n/a, 2004. B06201.

[105] I. Jackson, J. D. Fitz Gerald, U. H. Fau, and B. H. Tan. Grain-size-sensitive seismic wave attenuation in polycrystalline olivine. *Journal of Geophysical Research: Solid Earth*, 107(B12):ECV 5–1–ECV 5–16, 2002. 2360.

[106] R. Jaumann, K. Stephan, G. B. Hansen, R. N. Clark, B. J. Buratti, R. H. Brown, K. H. Baines, S. F. Newman, G. Bellucci, G. Filacchione, A. Coradini, D. P. Cruikshank, C. A. Griffith, C. A. Hibbitts, T. B. McCord, R. M. Nelson, P. D. Nicholson, C. Sotin, and R. Wagner. Distribution of icy particles across Enceladus' surface as derived from Cassini-VIMS measurements. *Icarus*, 193:407–419, February 2008.

[107] D. C. Jewitt and J. Luu. Crystalline water ice on the Kuiper belt object (50000) Quaoar. *Nature*, 432:731–733, December 2004.

[108] A. Juhász and M. Horányi. Saturn's E ring: A dynamical approach. *Journal of Geophysical Research (Space Physics)*, 107:1066, June 2002.

[109] S. Karato and H. A. Spetzler. Defect microdynamics in minerals and solid-state mechanisms of seismic wave attenuation and velocity dispersion in the mantle. *Reviews of Geophysics*, 28(4):399–421, 1990.

[110] J. S. Kargel. Ammonia-water volcanism on icy satellites - Phase relations at 1 atmosphere. *Icarus*, 100:556–574, December 1992.

[111] J. S Kargel. *Mars-A warmer, wetter planet*. Springer Science & Business Media, 2004.

[112] H. Kawakita and J.-i. Watanabe. Revised Fluorescence Efficiencies of Cometary NH_2: Ammonia Abundance in Comets. *The Astrophysical Journal*, 572:L177–L180, June 2002.

[113] S. Kempf, U. Beckmann, and J. Schmidt. How the Enceladus dust plume feeds Saturn's E ring. *Icarus*, 206:446–457, April 2010.

[114] L. Keszthelyi, W. Jaeger, M. Milazzo, J. Radebaugh, A. G. Davies, and K. L. Mitchell. New estimates for Io eruption temperatures: Implications for the interior. *Icarus*, 192(2):491 – 502, 2007.

[115] S. W. Kieffer, R. Lopes-Gautier, A. McEwen, W. Smythe, L. Keszthelyi, and R. Carlson. Prometheus: Io's Wandering Plume. *Science*, 288:1204–1208, May 2000.

[116] S. W. Kieffer, X. Lu, C. M. Bethke, J. R. Spencer, S. Marshak, and A. Navrotsky. A Clathrate Reservoir Hypothesis for Enceladus' South Polar Plume. *Science*, 314:1764, December 2006.

[117] M. T. Kirchner, R. Boese, W. E. Billups, and L. R. Norman. Gas hydrate single-crystal structure analyses. *Journal of the American Chemical Society*, 126(30):9407–9412, 2004. PMID: 15281833.

[118] M. R. Kirchoff and P. Schenk. Crater modification and geologic activity in Enceladus' heavily cratered plains: Evidence from the impact crater distribution. *Icarus*, 202:656–668, August 2009.

[119] J. Klinger. Influence of a phase transition of ice on the heat and mass balance of comets. *Science*, 209:271, July 1980.

[120] A. Kouchi and T. Kuroda. Amorphization of cubic ice by ultraviolet irradiation. *Nature*, 344:134, March 1990.

[121] A. Kouchi, T. Yamamoto, T. Kozasa, T. Kuroda, and J. M. Greenberg. Conditions for condensation and preservation of amorphous ice and crystallinity of astrophysical ices. *Astronomy and Astrophysics*, 290:1009–1018, October 1994.

[122] V. A. Krasnopolsky. Middle Ultraviolet Spectroscopy of Pluto and Charon. *Icarus*, 153:277–284, October 2001.

[123] V. Lainey, Ö. Karatekin, J. Desmars, S. Charnoz, J.-E. Arlot, N. Emelyanov, C. Le Poncin-Lafitte, S. Mathis, F. Remus, G. Tobie, and J.-P. Zahn. Strong Tidal Dissipation in Saturn and Constraints on Enceladus' Thermal State from Astrometry. *The Astrophysical Journal*, 752:14, June 2012.

[124] T. E. Leftwich, R. R. B. von Frese, H. R. Kim, H. C. Noltimier, L. V. Potts, D. R. Roman, and L. Tan. Crustal analysis of Venus from Magellan satellite observations at Atalanta Planitia, Beta Regio, and Thetis Regio. *Journal of Geophysical Research*, 104:8441–8462, April 1999.

[125] G. Leto and G. A. Baratta. Ly-alpha photon induced amorphization of Ic water ice at 16 K. Effects and quantitative comparison with ion irradiation. *Astronomy and Astrophysics*, 397:7–13, January 2003.

[126] G. Leto, O. Gomis, and G. Strazzulla. The reflectance spectrum of water ice: Is the 1.65 μm peak a good temperature probe?. *Memorie della Societa Astronomica Italiana Supplementi*, 6:57, 2005.

[127] J. S. Lewis. *Physics and chemistry of the solar system.* 1997.

[128] J. S. Lewis and R. G. Prinn. Planets and their atmospheres - Origin and evolution. *Orlando FL Academic Press Inc International Geophysics Series*, 33, 1984.

[129] K. Lodders. Solar System Abundances and Condensation Temperatures of the Elements. *The Astrophysical Journal*, 591:1220–1247, July 2003.

[130] R. Lopes. The rampant volcanoes of Io. *Planetary Science Report*, pages 6–11, 2002.

[131] R. M. C. Lopes, R. L. Kirk, K. L. Mitchell, A. Legall, J. W. Barnes, A. Hayes, J. Kargel, L. Wye, J. Radebaugh, E. R. Stofan, M. A. Janssen, C. D. Neish, S. D. Wall, C. A. Wood, J. I. Lunine, and M. J. Malaska. Cryovolcanism on Titan: New results from Cassini RADAR and VIMS. *Journal of Geophysical Research (Planets)*, 118:416–435, March 2013.

[132] R. M. C. Lopes, K. L. Mitchell, E. R. Stofan, J. I. Lunine, R. Lorenz, F. Paganelli, R. L. Kirk, C. A. Wood, S. D. Wall, L. E. Robshaw, A. D. Fortes, C. D. Neish, J. Radebaugh, E. Reffet, S. J. Ostro, C. Elachi, M. D. Allison, Y. Anderson, R. Boehmer, G. Boubin, P. Callahan, P. Encrenaz, E. Flamini, G. Francescetti, Y. Gim, G. Hamilton, S. Hensley, M. A. Janssen, W. T. K. Johnson, K. Kelleher, D. O. Muhleman, G. Ori, R. Orosei, G. Picardi, F. Posa, L. E. Roth, R. Seu, S. Shaffer, L. A. Soderblom, B. Stiles, S. Vetrella, R. D. West, L. Wye, and H. A. Zebker. Cryovolcanic features on Titan's surface as revealed by the Cassini Titan Radar Mapper. *Icarus*, 186:395–412, February 2007.

[133] R. M. C. Lopes, K. L. Mitchell, D. A. Williams, and G. Mitri. Beyond earth: How extra-terrestrial volcanism has changed our definition of a volcano. In E. Canon and A. Szakacs, editors, *What's a Volcano? New Answers to an Old Question*, pages 11–30. Geological Society of America, Inc., Boulder, Colo., 2010.

[134] R. M. C. Lopes, E. R. Stofan, R. Peckyno, J. Radebaugh, K. L. Mitchell, G. Mitri, C. A. Wood, R. L. Kirk, S. D. Wall, J. I. Lunine, A. Hayes, R. Lorenz, T. Farr,

L. Wye, J. Craig, R. J. Ollerenshaw, M. Janssen, A. Legall, F. Paganelli, R. West, B. Stiles, P. Callahan, Y. Anderson, P. Valora, L. Soderblom, and The Cassini Radar Team. Distribution and interplay of geologic processes on Titan from Cassini RADAR data. *Icarus*, 205:540–558, feb 2010a.

[135] R. D. Lorenz. Pillow lava on Titan: expectations and constraints on cryovolcanic processes. *Planetary and Space Science*, 44:1021–1028, September 1996.

[136] R. D. Lorenz and S. E. Shandera. Physical properties of ammonia-rich ice: Application to Titan. *Geophysical Research Letters*, 28:215–218, 2001.

[137] A. E. H. Love. *A treatise on the mathematical theory of elasticity.* University Press, 1892.

[138] R. Malhotra. Tidal origin of the Laplace resonance and the resurfacing of Ganymede. *Icarus*, 94(2):399 – 412, 1991.

[139] M. Manga and C. Y. Wang. Pressurized oceans and the eruption of liquid water on Europa and Enceladus. *Geophysical Research Letters*, 34:L07202, April 2007.

[140] F. Marchis, I. de Pater, A. G. Davies, H. G. Roe, T. Fusco, D. Le Mignant, P. Descamps, B. A. Macintosh, and R. Prangé. High-Resolution Keck Adaptive Optics Imaging of Violent Volcanic Activity on Io. *Icarus*, 160:124–131, November 2002.

[141] G. M. Marion, J. S. Kargel, D. C. Catling, and J. I. Lunine. Modeling ammonia-ammonium aqueous chemistries in the Solar System's icy bodies. *Icarus*, 220:932–946, August 2012.

[142] J. V. Martonchik, G. S. Orton, and J. F. Appleby. Optical properties of NH3 ice from the far infrared to the near ultraviolet. *Applied Optics*, 23:541–547, February 1984.

[143] R. M. Mastrapa, M. P. Bernstein, and S. A. Sandford. Near Infrared Spectra of H_2O/HCN Mixtures. In S. Mackwell and E. Stansbery, editors, *37th Annual Lunar and Planetary Science Conference*, volume 37 of *Lunar and Planetary Inst. Technical Report*, March 2006.

[144] R. M. E. Mastrapa and R. H. Brown. Ion irradiation of crystalline H_2O-ice: Effect on the 1.65-μm band. *Icarus*, 183:207–214, July 2006.

[145] D. L. Matson and R. H. Brown. Solid-state greenhouses and their implications for icy satellites. *Icarus*, 77:67–81, January 1989.

[146] D. L. Matson, J. C. Castillo-Rogez, A. G. Davies, and T. V. Johnson. Enceladus: A hypothesis for bringing both heat and chemicals to the surface. *Icarus*, 221:53–62, September 2012.

[147] C. McCarthy and J. C. Castillo-Rogez. Springer, New York, 2013.

[148] C. McCarthy, D. L. Goldsby, R. F. Cooper, W. B. Durham, and S. H. Kirby. Steady-State Creep Respose of Ice-I/Magnesium Sulfate Hydrate. In *Workshop on Ices, Oceans, and Fire: Satellites of the Outer Solar System*, volume 1357 of *LPI Contributions*, pages 88–89, August 2007.

[149] T. B. McCord, G. B. Hansen, F. P. Fanale, R. W. Carlson, D. L. Matson, T. V. Johnson, W. D. Smythe, J. K. Crowley, P. D. Martin, A. Ocampo, C. A. Hibbitts, and J. C. Granahan. Salts on Europa's Surface Detected by Galileo's Near Infrared Mapping Spectrometer. *Science*, 280:1242, May 1998.

[150] A. S. McEwen, M. J. S. Belton, H. H. Breneman, S. A. Fagents, P. Geissler, R. Greeley, J. W. Head, G. Hoppa, W. L. Jaeger, T. V. Johnson, L. Keszthelyi, K. P. Klaasen, R. Lopes-Gautier, K. P. Magee, M. P. Milazzo, J. M. Moore, R. T. Pappalardo, C. B. Phillips, J. Radebaugh, G. Schubert, P. Schuster, D. P. Simonelli, R. Sullivan, P. C. Thomas, E. P. Turtle, and D. A. Williams. Galileo at Io: Results from High-Resolution Imaging. *Science*, 288:1193–1198, May 2000.

[151] A. S. McEwen, L. Keszthelyi, J. R. Spencer, G. Schubert, D. L. Matson, R. Lopes-Gautier, K. P. Klaasen, T. V. Johnson, J. W. Head, P. Geissler, S. Fagents, A. G. Davies, M. H. Carr, H. H. Breneman, and M. J. S. Belton. High-temperature silicate volcanism on Jupiter's moon Io. *Science*, 281(5373):87–90, 1998.

[152] W. B. McKinnon. *Midsize Icy Satellites*, page 297. 1999.

[153] W. B. McKinnon. The Shape of Enceladus' Core: Predictions for Degree-2 Non-hydrostatic Gravity, and Role in Survival of the Subsurface Ocean. In *EPSC-DPS Joint Meeting 2011*, page 1572, October 2011.

[154] J. Meyer and J. Wisdom. Tidal heating in Enceladus. *Icarus*, 188:535–539, June 2007.

[155] J. Meyer and J. Wisdom. Tidal evolution of Mimas, Enceladus, and Dione. *Icarus*, 193:213–223, January 2008a.

[156] J. Meyer and J. Wisdom. Episodic volcanism on Enceladus: Application of the Ojakangas Stevenson model. *Icarus*, 198:178–180, November 2008b.

[157] G. Mitri and A. P. Showman. A model for the temperature-dependence of tidal dissipation in convective plumes on icy satellites: Implications for Europa and Enceladus. *Icarus*, 195:758–764, June 2008.

[158] G. Mitri, A. P. Showman, J. I. Lunine, and R. M. C. Lopes. Resurfacing of Titan by ammonia-water cryomagma. *Icarus*, 196:216–224, July 2008.

[159] J. M. Moore and R. T. Pappalardo. Titan: An exogenic world? *Icarus*, 212:790–806, April 2011.

[160] M. H. Moore and R. L. Hudson. Far-infrared spectral studies of phase changes in water ice induced by proton irradiation. *Astrophysical Journal*, 401:353–360, December 1992.

[161] W. B. Moore. Tidal heating and convection in Io. *Journal of Geophysical Research: Planets*, 108(E8):n/a–n/a, 2003. 5096.

[162] W. B. Moore and H. Hussmann. Thermal evolution of Europa's silicate interior. In *Europa*, Tucson, 2009. University of Arizona Press.

[163] L. A. Morabito, S. P. Synnott, P. N. Kupferman, and S. A. Collins. Discovery of currently active extraterrestrial volcanism. *Science*, 204(4396):972–972, 1979.

[164] M. W. Morooka, J.-E. Wahlund, A. I. Eriksson, W. M. Farrell, D. A. Gurnett, W. S. Kurth, A. M. Persoon, M. Shafiq, M. André, and M. K. G. Holmberg. Dusty plasma in the vicinity of Enceladus. *Journal of Geophysical Research (Space Physics)*, 116:A12221, December 2011.

[165] I. Mosqueira, P. Estrada, and D. Turrini. Planetesimals and Satellitesimals: Formation of the Satellite Systems. *Space Science Reviews*, 153:431–446, June 2010.

[166] C. D. Murray and S. F. Dermott. *Solar system dynamics*. 1999.

[167] S. F. Newman, B. J. Buratti, R. H. Brown, R. Jaumann, J. Bauer, and T. Momary. Photometric and spectral analysis of the distribution of crystalline and amorphous ices on Enceladus as seen by Cassini. *Icarus*, 193:397–406, February 2008.

[168] S. F. Newman, B. J. Buratti, R. Jaumann, J. M. Bauer, and T. W. Momary. Hydrogen Peroxide on Enceladus. *The Astrophysical Journal*, 670:L143–L146, December 2007.

[169] F. Nimmo and D. McKenzie. Volcanism and Tectonics on Venus. *Annual Review of Earth and Planetary Sciences*, 26:23–53, 1998.

[170] F. Nimmo and R. T. Pappalardo. Diapir-induced reorientation of Saturn's moon Enceladus. *Nature*, 441:614–616, June 2006.

[171] F. Nimmo, J. R. Spencer, R. T. Pappalardo, and M. E. Mullen. Shear heating as the origin of the plumes and heat flux on Enceladus. *Nature*, 447:289–291, May 2007.

[172] F. Nimmo and D. J. Stevenson. Influence of early plate tectonics on the thermal evolution and magnetic field of mars. *Journal of Geophysical Research: Planets*, 105(E5):11969–11979, 2000.

[173] R. J. O'Connell and B. Hager. ed. A. M. Dziewonski and E. Boschi (North Holland: Elsevier), 1980.

[174] M. Ogihara and S. Ida. N-body Simulations of Satellite Formation around Giant Planets: Origin of Orbital Configuration of the Galilean Moons. *The Astrophysical Journal*, 753:60, July 2012.

[175] G. W. Ojakangas and D. J. Stevenson. Episodic volcanism of tidally heated satellites with application to Io. *Icarus*, 66:341–358, May 1986.

[176] C. O'Neill and F. Nimmo. The role of episodic overturn in generating the surface geology and heat flow on Enceladus. *Nature Geoscience*, 3:88–91, February 2010.

[177] T. Owen. *Titan*, page 277. 1999.

[178] F. Paganelli, M.A. Janssen, R.M. Lopes, E. Stofan, S.D. Wall, R.D. Lorenz, J.I. Lunine, R.L. Kirk, L. Roth, and C. Elachi. Titan's surface from the Cassini RADAR radiometry data during SAR mode. *Planetary and Space Science*, 56(1):100 – 108, 2008. Surfaces and Atmospheres of the Outer Planets, their Satellites and Ring Systems: Part III.

[179] R. T. Pappalardo. *Ganymede and Callisto*, page 263. 1999.

[180] R. T. Pappalardo. Miranda: Shattering an image. *The Planetary Report*, pages 14–18, 2005.

[181] R. T. Pappalardo, M. J. S. Belton, H. H. Breneman, M. H. Carr, C. R. Chapman, G. C. Collins, T. Denk, S. Fagents, P. E. Geissler, B. Giese, R. Greeley, R. Greenberg, J. W. Head, P. Helfenstein, G. Hoppa, S. D. Kadel, K. P. Klaasen, J. E. Klemaszewski, K. Magee, A. S. McEwen, J. M. Moore, W. B. Moore, G. Neukum, C. B. Phillips, L. M. Prockter, G. Schubert, D. A. Senske, R. J. Sullivan, B. R. Tufts, E. P. Turtle, R. Wagner, and K. K. Williams. Does Europa have a subsurface ocean? Evaluation of the geological evidence. *Journal of Geophysical Research*, 104:24015–24056, October 1999.

[182] D. A. Patthoff and S. A. Kattenhorn. A fracture history on Enceladus provides evidence for a global ocean. *Geophysical Research Letters*, 38:L18201, September 2011.

[183] S. J. Peale and P. Cassen. Contribution of tidal dissipation to lunar thermal history. *Icarus*, 36(2):245 – 269, 1978.

[184] S. J. Peale and M. H. Lee. A primordial origin of the Laplace relation among the Galilean Satellites. *Science*, 298(5593):593–597, 2002.

[185] C. Porco, D. DiNino, and F. Nimmo. How the Jets, Heat and Tidal Stresses Across the South Polar Terrain of Enceladus are Related. In *Lunar and Planetary Science Conference*, volume 44 of *Lunar and Planetary Inst. Technical Report*, page 1775, March 2013.

[186] C. C. Porco, P. Helfenstein, P. C. Thomas, A. P. Ingersoll, J. Wisdom, R. West, G. Neukum, T. Denk, R. Wagner, T. Roatsch, S. Kieffer, E. Turtle, A. McEwen, T. V. Johnson, J. Rathbun, J. Veverka, D. Wilson, J. Perry, J. Spitale, A. Brahic, J. A. Burns, A. D. Del Genio, L. Dones, C. D. Murray, and S. Squyres. Cassini Observes the Active South Pole of Enceladus. *Science*, 311:1393–1401, March 2006.

[187] F. Postberg, S. Kempf, J. Schmidt, N. Brilliantov, A. Beinsen, B. Abel, U. Buck, and R. Srama. Sodium salts in E-ring ice grains from an ocean below the surface of Enceladus. *Nature*, 459:1098–1101, June 2009.

[188] F. Postberg, J. Schmidt, J. Hillier, S. Kempf, and R. Srama. A salt-water reservoir as the source of a compositionally stratified plume on Enceladus. *Nature*, 474:620–622, June 2011.

[189] L. Prockter. Ice volcanism on Jupiters moons and beyond. In R. Lopes and T. K. Gregg, editors, *Volcanic Worlds: Exploring the Solar System Volcanoes*. Praxis Publishing Company (Springer-Verlag), 2004.

[190] W. R. Pryor, A. M. Rymer, D. G. Mitchell, T. W. Hill, D. T. Young, J. Saur, G. H. Jones, S. Jacobsen, S. W. H. Cowley, B. H. Mauk, A. J. Coates, J. Gustin, D. Grodent, J.-C. Gérard, L. Lamy, J. D. Nichols, S. M. Krimigis, L. W. Esposito, M. K. Dougherty, A. J. Jouchoux, A. I. F. Stewart, W. E. McClintock, G. M. Holsclaw, J. M. Ajello, J. E. Colwell, A. R. Hendrix, F. J. Crary, J. T. Clarke, and X. Zhou. The auroral footprint of Enceladus on Saturn. *Nature*, 472:331–333, April 2011.

[191] J. Radebaugh, R. D. Lorenz, S. D. Wall, R. L. Kirk, C. A. Wood, J. I. Lunine, E. R. Stofan, R. M. C. Lopes, P. Valora, T. G. Farr, A. Hayes, B. Stiles, G. Mitri, H. Zebker, M. Janssen, L. Wye, A. LeGall, K. L. Mitchell, F. Paganelli, R. D. West, E. L. Schaller, and Cassini Radar Team. Regional geomorphology and history of Titan's Xanadu province. *Icarus*, 211:672–685, jan 2011.

[192] N. J. Rappaport, L. Iess, J. Wahr, J. I. Lunine, J.W. Armstrong, S. W. Asmar, . Tortora, M. Di Benedetto, and P. Racioppa. Can cassini detect a subsurface ocean in titan from gravity measurements? *Icarus*, 194(2):711 – 720, 2008.

[193] J. P. Renaud and W. G. Henning. Increased Tidal Dissipation using Realistic Rheological Models: Implications for the Thermal History of Io and Tidally Active Extrasolar Planets. *ArXiv e-prints*, July 2017.

[194] J. H. Roberts and F. Nimmo. Tidal heating and the long-term stability of a subsurface ocean on Enceladus. *Icarus*, 194:675–689, April 2008a.

[195] J. H. Roberts and F. Nimmo. Near-surface heating on Enceladus and the south polar thermal anomaly. *Geophysical Research Letters*, 35:L09201, May 2008b.

[196] M. S. Robinson and P. G. Lucey. Recalibrated Mariner 10 color mosaics: Implications for mercurian volcanism. *Science*, 275:197–200, 1997.

[197] R. G. Ross and J. S. Kargel. Thermal Conductivity of Solar System Ices, with Special Reference to Martian Polar Caps. In B. Schmitt, C. de Bergh, and M. Festou, editors, *Solar System Ices*, volume 227 of *Astrophysics and Space Science Library*, page 33, 1998.

[198] K. Röttger, A. Endriss, J. Ihringer, S. Doyle, and W. F. Kuhs. *Acta Crystallographica Section B*, 50(6):644–648, Dec 1994.

[199] F. Rouleau and P. G. Martin. Shape and clustering effects on the optical properties of amorphous carbon. *Astrophysical Journal*, 377:526–540, August 1991.

[200] T. L. Roush. Optical constants of amorphous water ice in the near-infrared. In *Lunar and Planetary Science Conference*, volume 28 of *Lunar and Planetary Inst. Technical Report*, page 199, March 1997.

[201] P. Saxena, J. P. Renaud, W. G. Henning, M. Jutzi, and T. Hurford. Relevance of tidal heating on large TNOs. *Icarus*, 302:245–260, March 2018.

[202] P. Schenk, D. P. Hamilton, R. E. Johnson, W. B. McKinnon, C. Paranicas, J. Schmidt, and M. R. Showalter. Plasma, plumes and rings: Saturn system dynamics as recorded in global color patterns on its midsize icy satellites. *Icarus*, 211:740–757, January 2011.

[203] P. M. Schenk and W. B. McKinnon. One-hundred-km-scale basins on Enceladus: Evidence for an active ice shell. *Geophysical Research Letters*, 36:L16202, August 2009.

[204] J. Schmidt, N. Brilliantov, F. Spahn, and S. Kempf. Slow dust in Enceladus' plume from condensation and wall collisions in tiger stripe fractures. *Nature*, 451:685–688, February 2008.

[205] B. Schmitt, E. Quirico, F. Trotta, and W. M. Grundy. Optical Properties of Ices from UV to Infrared. In B. Schmitt, C. de Bergh, and M. Festou, editors, *Solar System Ices*, volume 227 of *Astrophysics and Space Science Library*, page 199, 1998.

[206] N. M. Schneider, M. H. Burger, E. L. Schaller, M. E. Brown, R. E. Johnson, J. S. Kargel, M. K. Dougherty, and N. A. Achilleos. No sodium in the vapour plumes of Enceladus. *Nature*, 459:1102–1104, June 2009.

[207] G. Schubert, J. D. Anderson, B. J. Travis, and J. Palguta. Enceladus: Present internal structure and differentiation by early and long-term radiogenic heating. *Icarus*, 188:345–355, June 2007.

[208] M. Segatz, T. Spohn, M.N. Ross, and G. Schubert. Tidal dissipation, surface heat flow, and figure of viscoelastic models of Io. *Icarus*, 75(2):187 – 206, 1988.

[209] D. E. Shemansky, P. Matheson, D. T. Hall, H.-Y. Hu, and T. M. Tripp. Detection of the hydroxyl radical in the Saturn magnetosphere. *Nature*, 363:329–331, May 1993.

[210] D. Shoji and K. Kurita. Thermal-orbital coupled tidal heating and habitability of martian-sized extrasolar planets around M stars. *The Astrophysical Journal*, 789(1):3, 2014.

[211] A. P. Showman and R. Malhotra. Tidal evolution into the Laplace resonance and the resurfacing of Ganymede. *Icarus*, 127(1):93 – 111, 1997.

[212] A. P. Showman, I. Mosqueira, and J. W. Head. On the resurfacing of Ganymede by liquid water volcanism. *Icarus*, 172:625–640, December 2004.

[213] L. M. Shulman. The heat capacity of water ice in interstellar or interplanetary conditions. *Astronomy and Astrophysics*, 416:187–190, March 2004.

[214] B. Sicardy, A. Bellucci, E. Gendron, F. Lacombe, S. Lacour, J. Lecacheux, E. Lellouch, S. Renner, S. Pau, F. Roques, T. Widemann, F. Colas, F. Vachier, R. V. Martins, N. Ageorges, O. Hainaut, O. Marco, W. Beisker, E. Hummel, C. Feinstein, H. Levato, A. Maury, E. Frappa, B. Gaillard, M. Lavayssière, M. di Sora, F. Mallia, G. Masi, R. Behrend, F. Carrier, O. Mousis, P. Rousselot, A. Alvarez-Candal, D. Lazzaro, C. Veiga, A. H. Andrei, M. Assafin, D. N. da Silva Neto, C. Jacques, E. Pimentel, D. Weaver, J.-F. Lecampion, F. Doncel, T. Momiyama, and G. Tancredi. Charon's size and an upper limit on its atmosphere from a stellar occultation. *Nature*, 439:52–54, January 2006.

[215] D. E. Smith, M. T. Zuber, and G. A. Neumann. Seasonal Variations of Snow Depth on Mars. *Science*, 294:2141–2146, December 2001.

[216] L. A. Soderblom, R. H. Brown, J. M. Soderblom, J. W. Barnes, R. L. Kirk, C. Sotin, R. Jaumann, D. J. Mackinnon, D. W. Mackowski, K. H. Baines, B. J. Buratti, R. N. Clark, and P. D. Nicholson. The geology of Hotei Regio, Titan: Correlation of Cassini VIMS and RADAR. *Icarus*, 204:610–618, December 2009.

[217] F. Sohl. Revealing titan's interior. *Science*, 327(5971):1338–1339, 2010.

[218] F. Sohl and T. Spohn. The interior structure of Mars: Implications from SNC meteorites. *Journal of Geophysical Research*, 102:1613–1636, January 1997.

[219] C. Sotin, J. W. Head, and G. Tobie. Europa: Tidal heating of upwelling thermal plumes and the origin of lenticulae and chaos melting. *Geophysical Research Letters*, 29:1233, April 2002.

[220] J. R. Spencer. The Thermal Inertias of Rhea, Dione, and Tethys from Ground-based Radiometry. In *Bulletin of the American Astronomical Society*, volume 21 of *Bulletin of the American Astronomical Society*, page 983, June 1989.

[221] J. R. Spencer, A. C. Barr, L. W. Esposito, P. Helfenstein, A. P. Ingersoll, R. Jaumann, C. P. McKay, F. Nimmo, and J. H. Waite. *Enceladus: An Active Cryovolcanic Satellite*, page 683. 2009.

[222] J. R. Spencer, C. J. A. Howett, A. J. Verbiscer, T. A. Hurford, M. E. Segura, and J. C. Pearl. High-Resolution Observations of Thermal Emission from the South Pole of Enceladus. In *Lunar and Planetary Science Conference*, volume 42 of *Lunar and Planetary Inst. Technical Report*, page 2553, March 2011.

[223] J. R. Spencer, K. L. Jessup, M. A. McGrath, G. E. Ballester, and R. Yelle. Discovery of Gaseous S_2 in Io's Pele Plume. *Science*, 288:1208–1210, May 2000.

[224] J. R. Spencer, L. A. Lebofsky, and M. V. Sykes. Systematic biases in radiometric diameter determinations. *Icarus*, 78:337–354, April 1989.

[225] J. R. Spencer and J. M. Moore. The influence of thermal inertia on temperatures and frost stability on Triton. *Icarus*, 99:261–272, October 1992.

[226] J. R. Spencer and F. Nimmo. Enceladus: An Active Ice World in the Saturn System. *Annual Review of Earth and Planetary Sciences*, 41:693–717, May 2013.

[227] J. R. Spencer, J. C. Pearl, M. Segura, F. M. Flasar, A. Mamoutkine, P. Romani, B. J. Buratti, A. R. Hendrix, L. J. Spilker, and R. M. C. Lopes. Cassini Encounters Enceladus: Background and the Discovery of a South Polar Hot Spot. *Science*, 311:1401–1405, March 2006.

[228] J. R. Spencer, S. A. Stern, A. F. Cheng, H. A. Weaver, D. C. Reuter, K. Retherford, A. Lunsford, J. M. Moore, O. Abramov, R. M. C. Lopes, J. E. Perry, L. Kamp, M. Showalter, K. L. Jessup, F. Marchis, P. M. Schenk, and C. Dumas. Io volcanism seen by New Horizons: A major eruption of the Tvashtar volcano. *Science*, 318(5848):240–243, 2007.

[229] J. R. Spencer, L. K. Tamppari, T. Z. Martin, and L. D. Travis. Temperatures on Europa from Galileo Photopolarimeter-Radiometer: Nighttime Thermal Anomalies. *Science*, 284:1514, May 1999.

[230] J. N. Spitale and C. C. Porco. Association of the jets of Enceladus with the warmest regions on its south-polar fractures. *Nature*, 449:695–697, October 2007.

[231] D. J. Stevenson. Limits on the Variation of Thickness of Europa's Ice Shell. In *Lunar and Planetary Science Conference*, volume 31 of *Lunar and Planetary Inst. Technical Report*, March 2000.

[232] G. Strazzulla, G. A. Baratta, G. Leto, and G. Foti. Ion-beam-induced amorphization of crystalline water ice. *EPL (Europhysics Letters)*, 18:517, March 1992.

[233] G. Strazzulla and M. E. Palumbo. Evolution of icy surfaces : an experimental approach. *Planetary and Space Science*, 46:1339–1348, October 1998.

[234] R. G. Strom, G. G. Schaber, and D. D. Dawson. The Global Resurfacing History of Venus. In *Lunar and Planetary Science Conference*, volume 25 of *Lunar and Planetary Inst. Technical Report*, page 1353, March 1994.

[235] M. Sundberg and R. F. Cooper. A composite viscoelastic model for incorporating grain boundary sliding and transient diffusion creep; correlating creep and attenuation responses for materials with a fine grain size. *Philosophical Magazine*, 90(20):2817–2840, 2010.

[236] I. M. Taban, W. A. Schutte, K. M. Pontoppidan, and E. F. van Dishoeck. Stringent upper limits to the solid NH_3 abundance towards W 33A from near-IR spectroscopy with the Very Large Telescope. *Astronomy and Astrophysics*, 399:169–175, February 2003.

[237] E. Takahashi. Speculations on the archean mantle: Missing link between komatiite and depleted garnet peridotite. *Journal of Geophysical Research: Solid Earth*, 95(B10):15941–15954, 1990.

[238] S. R. Taylor. *Solar system evolution: a new perspective. an inquiry into the chemical composition, origin, and evolution of the solar system.* 1992.

[239] K.-U. Thiessenhusen, A. V. Krivov, H. Krüger, and E. Grün. A dust cloud around Pluto and Charon. *Planetary and Space Science*, 50:79–87, January 2002.

[240] P. C. Thomas. Sizes, shapes, and derived properties of the saturnian satellites after the Cassini nominal mission. *Icarus*, 208:395–401, July 2010.

[241] G. Tobie, O. Grasset, J. I. Lunine, A. Mocquet, and C. Sotin. Titan's internal structure inferred from a coupled thermal-orbital model. *Icarus*, 175(2):496 – 502, 2005.

[242] G. Tobie, O. Čadek, and C. Sotin. Solid tidal friction above a liquid water reservoir as the origin of the south pole hotspot on Enceladus. *Icarus*, 196:642–652, August 2008.

[243] D. L. Turcotte. Magellan, Venus, and the Earth. In *Lunar and Planetary Science Conference*, volume 26 of *Lunar and Planetary Inst. Technical Report*, March 1995.

[244] R. Tyler. Tidal dynamical considerations constrain the state of an ocean on Enceladus. *Icarus*, 211:770–779, January 2011.

[245] A. Verbiscer, R. French, M. Showalter, and P. Helfenstein. Enceladus: Cosmic Graffiti Artist Caught in the Act. *Science*, 315:815, February 2007.

[246] J. H. Waite, B. Magee, T. Brockwell, M. Y. Zolotov, B. Teolis, and W. S. Lewis. Enceladus Plume Composition. In *EPSC-DPS Joint Meeting 2011*, page 61, October 2011.

[247] J. H. Waite, Jr., W. S. Lewis, B. A. Magee, J. I. Lunine, W. B. McKinnon, C. R. Glein, O. Mousis, D. T. Young, T. Brockwell, J. Westlake, M.-J. Nguyen, B. D. Teolis, H. B. Niemann, R. L. McNutt, M. Perry, and W.-H. Ip. Liquid water on Enceladus from observations of ammonia and ^{40}Ar in the plume. *Nature*, 460:487–490, July 2009.

[248] S. D. Wall, R. M. Lopes., E. R. Stofan, C. A. Wood, J. L. Radebaugh, S. M. Hörst, B. W. Stiles, R. M. Nelson, L. W. Kamp, M. A. Janssen, R. D. Lorenz, J. I. Lunine, T. G. Farr, G. Mitri, P. Paillou, F. Paganelli, and K. L. Mitchell. Cassini RADAR images at Hotei Arcus and western Xanadu, Titan: Evidence for geologically recent cryovolcanic activity. *Geophysical Research Letters*, 36:L04203, February 2009.

[249] S. G. Warren. Optical constants of ice from the ultraviolet to the microwave. *Applied Optics*, 23:1206–1225, April 1984.

[250] S. Webb and I. Jackson. Anelasticity and microcreep in polycrystalline MgO at high temperature: an exploratory study. *Physics and Chemistry of Minerals*, 30(3):157–166, Apr 2003.

[251] J. Weertman and J. R. Weertman. High temperature creep of rock and mantle viscosity. *Annual Review of Earth and Planetary Sciences*, 3(1):293–315, 1975.

[252] P. R. Weissman, L.-A. McFadden, and T. V. Johnson. *Encyclopedia of the solar system.* Academic Press San Diego, 1999.

[253] C. A. Wood. Bipolar Volcanism on Titan? In *Lunar and Planetary Science Conference*, volume 42 of *Lunar and Planetary Inst. Technical Report*, page 1313, March 2011.

[254] P. J. Wyllie. Experimental petrology: Earth materials science. In *Understanding the Earth; A New Synthesis*, pages 67–87. Cambridge University Press, Cambridge, 1992.

[255] C. F. Yoder. How tidal heating in Io drives the Galilean orbital resonance locks. *Nature*, 279:767–770, June 1979.

[256] C. F. Yoder, A. S. Konopliv, D. N. Yuan, E. M. Standish, and W. M. Folkner. Fluid Core Size of Mars from Detection of the Solar Tide. *Science*, 300:299–303, April 2003.

[257] C. F. Yoder and S. J. Peale. The tides of Io. *Icarus*, 47(1):1 – 35, 1981.

[258] C. F. Yoder and E. M. Standish. Martian precession and rotation from Viking lander range data. *Journal of Geophysical Research*, 102:4065–4080, 1997.

[259] K. Zahnle, P. Schenk, H. Levison, and L. Dones. Cratering rates in the outer Solar System. *Icarus*, 163:263–289, June 2003.

[260] K. Zhang and F. Nimmo. Recent orbital evolution and the internal structures of Enceladus and Dione. *Icarus*, 204:597–609, December 2009.

[261] V. N. Zharkov and T. V. Gudkova. Interior structure models, Fe/Si ratio and parameters of figure for Mars. *Physics of the Earth and Planetary Interiors*, 117:407–420, January 2000.

[262] M. Y. Zolotov. An oceanic composition on early and today's Enceladus. *Geophysical Research Letters*, 34:L23203, December 2007.